



Norwegian University of  
Science and Technology

# Wind Turbine in Yawed Operation

**Kari Medby Loland**

Master of Science in Energy and Environment

Submission date: June 2011

Supervisor: Per-Åge Krogstad, EPT

Norwegian University of Science and Technology  
Department of Energy and Process Engineering



EPT-M-2011-29

**MASTER THESIS**

for

**Stud.techn. Kari Medby Loland**

Spring 2011

Wind turbine in yawed operation

*Vindturbin med sidevind***Background and objective**

It is well known that if the rotor plane of a horizontal axis wind turbine is not perpendicular to the incoming flow, this will cause a loss in power production. This has, however, also other important implications which should be investigated. Because the flow is asymmetric, the wake generated by the rotor will also be asymmetric and will be deflected sideways as it drifts downstream. This may generate high loads on turbines downstream. In addition, the non-symmetric load will generate a turning moment on the rotor which produces forces which must be balanced by a braking system in the nacelle. This moment will depend on the yaw angle and the distance between the rotor plane and the tower. It is therefore expected to be different for upstream and downstream rotor layouts.

This investigation is primarily an experimental study and should be performed in the large wind tunnel on one of the wind turbine models available at the department.

The student should perform the following tasks:

- Learn the experimental techniques required to measure forces and moments on a model, as well as methods to measure the mean velocity in the flow
- With the model turbine mounted in the tunnel, forces and moments as function of yaw angle should be measured both for an upstream and downstream rotor configuration
- Determine the growth rate and path of the wake behind the rotor for some selected turbine operating conditions

-- " --

Within 14 days of receiving the written text on the master thesis, the candidate shall submit a research plan for his project to the department.

When the thesis is evaluated, emphasis is put on processing of the results, and that they are presented in tabular and/or graphic form in a clear manner, and that they are analyzed carefully.

The thesis should be formulated as a research report with summary both in English and Norwegian, conclusion, literature references, table of contents etc. During the preparation of the text, the candidate should make an effort to produce a well-structured and easily readable report. In order to ease the evaluation of the thesis, it is important that the cross-references are correct. In the making of the report, strong emphasis should be placed on both a thorough discussion of the results and an orderly presentation.

The candidate is requested to initiate and keep close contact with his/her academic supervisor(s) throughout the working period. The candidate must follow the rules and regulations of NTNU as well as passive directions given by the Department of Energy and Process Engineering.

Pursuant to "Regulations concerning the supplementary provisions to the technology study program/Master of Science" at NTNU §20, the Department reserves the permission to utilize all the results and data for teaching and research purposes as well as in future publications.

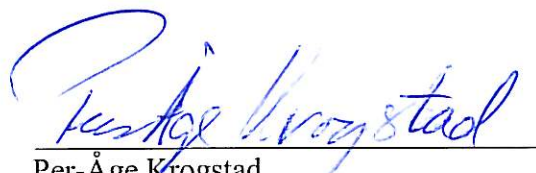
One – 1 complete original of the thesis shall be submitted to the authority that handed out the set subject. (A short summary including the author's name and the title of the thesis should also be submitted, for use as reference in journals (max. 1 page with double spacing)).

Two – 2 – copies of the thesis shall be submitted to the Department. Upon request, additional copies shall be submitted directly to research advisors/companies. A CD-ROM (Word format or corresponding) containing the thesis, and including the short summary, must also be submitted to the Department of Energy and Process Engineering

Department of Energy and Process Engineering, 10. January 2011



Olav Bolland  
Department Head



Per-Åge Krogstad  
Academic Supervisor

Research Advisors:

## PREFACE

This Master of Technology thesis was carried out at the Department of Energy and Process Engineering at the Norwegian University of Science and Technology (NTNU). The effect of yaw angle on the performance and wake behind a test turbine was tested in the wind tunnel at Strømningsteknisk laboratory. Measurements and completion of the thesis was done within 20 weeks, and gives 30 credit points.

The work with this thesis has been both challenging and informative. The frustrating task of doing experiments and finding that the results are not valid, has from time to time challenged my motivation. Still, when the problems were overcome the motivation always reappeared stronger than before.

Thanks to Professor Per-Åge Krogstad for helpful guidance and Pål Egil Eriksen for helping with his expertise in the field of performing wind tunnel experiments. Arnt Egil Kolstad has been helpful and patient in helping with the setup of equipment and heavy lifting, and my costudents has contributed with clarifying discussions on the way. Thanks to Muiwa S. Adaramola for supplying me his measurements for comparison.

Thanks to my dad for correcting my thesis even though his knowledge on the subject was limited, and thanks to my mum for her endless support.



Kari Medby Loland  
Trondheim, 14.06.2011



## ABSTRACT

The task of this project was to investigate the near wake, performance characteristics and yaw moment on a model wind turbine. The test turbine is a horizontal axis three bladed machine with a rotor diameter of 0.9 meter. Initially it is an upwind turbine, but was used for downwind measurements as well by rotating the blades and the entire construction  $180^\circ$ . For the wake measurements the tip speed ratio was set to be  $\lambda = 3$ ,  $\lambda = 6$  and  $\lambda = 9$  to describe the different regimes; partly stalled, optimal operation and partly propeller operation. Two different yaw angles,  $0^\circ$  and  $30^\circ$ , was also explored for the near wake measurements. The velocity field was measured at  $X/D = 1$ , as well as  $X/D = 4$  for  $\lambda = 6$  and the two yaw angles;  $X/D$  being the number of rotor diameters downstream from the rotor plane. The performance characteristics and yaw moment were measured for yaw angles  $0^\circ, 10^\circ, 20^\circ$  and  $30^\circ$ , and with tip speed ratios from 1 to 11.

The power and thrust coefficients were found to decrease with increasing yaw angle. This is due to the reduced projected rotor area and reduced effective wind velocity component interacting with the turbine blades. The loss in power due to the yaw angle of the turbine is approximately 6% for  $\gamma = 10^\circ$  and 40% for  $\gamma = 30^\circ$  with upstream configuration. For downstream setup the reduction in power due to the yaw angle was 5.2% and 38% for  $\gamma = 10^\circ$  and  $\gamma = 30^\circ$  respectively.

The near wake velocity field was strongly influenced by tip speed ratio and yaw angle. At  $\lambda \approx 3$  the outer parts of the wake had a velocity close to the freestream velocity. Therefore much of the flow passes through without interacting with the rotor blades. For  $\lambda \approx 6$  the velocity deficit was close to uniform in the wake. Most of the turbine blades operate efficiently at the design condition, and gives the peak in the power coefficient curve at this *TSR*. When  $\lambda \approx 9$  the inner part of the blades experience negative angle of attack and provide energy to the wind instead of subtracting it. The outer parts of the blade operate more efficiently, but due to the inner part working as a propeller the power coefficient is low. The thrust coefficient is high for this operating condition.

When the turbine is operating in yawed condition, the wake width is reduced and shifted towards the yawed direction. At downstream distance  $X/D = 4$  for  $\lambda \approx 6$  the wake deficit becomes more uniform for both  $\gamma = 0^\circ$  and  $\gamma = 30^\circ$ .

For the downstream configuration the yaw moment was generally stable at more operating conditions than the upstream setup. Common for both configurations was that the yaw moment tended to rotate the rotor plane out of the wind at low tip speed ratios and yaw angles. The downwind turbine got a stabilizing moment for a lower tip speed ratio than the upwind turbine for all yaw angles. Both upwind and downwind turbine setup had an unconditionally stable yaw moment for  $\gamma = 30^\circ$ .





## SAMMENDRAG

Målet med dette prosjektet var å undersøke nær-vake, ytelsesevne og dreiemoment til en test turbin. Vindturbinen er en horisontal akse konstruksjon med tre blader og en rotor diameter på  $0.9m$ . Det er i utgangspunktet en oppstrøms turbin, men er blitt brukt som nedstrøms turbin ved å rotere både blader og konstruksjon  $180^\circ$ . Vakemålinger er blitt utført for spiss hastigheter på  $\lambda = 3$ ,  $\lambda = 6$  og  $\lambda = 9$  for å beskrive tilfellene delvis stall på bladene, optimal drift og delvis propell funksjon. To ulike vinkler,  $0^\circ$  og  $30^\circ$ , er også undersøkt for nær-vake målingene. Hastighetsfeltet er målt ved  $X/D = 1$  og også  $X/D = 4$  for  $\lambda = 6$  og de to vinklene, der  $X/D$  er antall rotor diameter nedstrøms for rotorplanet. Ytelse og dreiemoment er målt for  $\gamma = 0^\circ, 10^\circ, 20^\circ$  og  $30^\circ$  med varierende spiss hastigheter fra 1 til 11.

Ved økende yaw vinkel, sank både effekt og thrust koeffisientene. Dette er grunnet redusert prosjektert rotor areal, og minket effektiv vin hastighetskomponent sett av bladene. Effekttap på oppstrøms vindturbin grunnet yaw vinkelen er 6% for  $\gamma = 10^\circ$  og 40% for  $\gamma = 30^\circ$  For en nedstrøms vindturbin ble effekttapene grunnet yaw funnet å være 5.2% og 38% for henholdsvis  $\gamma = 10^\circ$  og  $\gamma = 30^\circ$ .

Hastighetsfeltet i den nære vaken ble funnet å være sterkt avhengig av spiss hastighet og yaw vinkel. Ved  $\lambda \approx 3$  hadde de ytre delene av vaken en redusert hastighet som var svært lik fristrøms hastigheten. Grunnen til dette er at mye av strømmingen passerer turbinen uten å bli påvirket av rotorbladene. For en spiss hastighet på 6 var hastighetsreduksjonen i vaken nært uniformt fordelt. Store deler av turbinbladene opererer da effektivt ved designpunktet, og dette gir også den maksimale verdien for effektkoeffisienten. Når  $\lambda \approx 9$  opplever den indre delen av bladene en negativ angrepsvinkel. Dette gjør at turbinen tilfører energi til strømmingen i stede for å utnytte den. De ytre delene av bladene opererer mer effektivt, men effektkoeffisienten er lav grunnet at den indre delen opererer som en propell. Thrustkoeffisienten er høy for denne spiss hastigheten.

Når turbinen opererer i skjev innstrømning reduseres bredden til vaken, og den forskyves mot yaw retningen til turbinen. Vaken blir mer uniform for  $X/D = 4$  ved  $\lambda = 6$  for både  $\gamma = 0^\circ$  og  $\gamma = 30^\circ$ .

For nedstrøms konfigurasjon er dreiemomentet generelt mer stabiliserende for systemet enn for oppstrøms oppsett. Felles for begge situasjoner er at dreiemomentet søker å rotere rotor planet ut av vinden for lave yaw vinkler og spiss hastigheter. Forsøkene på nedstrøms turbin konfigurasjon fikk et stabiliserende moment ved lavere spiss hastighet enn oppstrøms oppsett for alle yaw vinkler. Både oppstrøms og nedstrøms konfigurering hadde betingelsesløst stabiliserende dreiemoment for  $\gamma = 30^\circ$ .



# Contents

<b>1</b>	<b>Introduction</b>	<b>2</b>
<b>2</b>	<b>Theory</b>	<b>4</b>
2.1	Wind turbine physics . . . . .	4
2.1.1	Forces and moments on a wind turbine . . . . .	4
2.1.2	Yaw angle . . . . .	7
2.2	Wind turbine wakes . . . . .	10
2.2.1	Wake expansion . . . . .	10
2.2.2	Wake rotation . . . . .	11
2.2.3	Wake with yaw angle . . . . .	12
<b>3</b>	<b>Experimental setup</b>	<b>13</b>
3.1	Wind tunnel . . . . .	13
3.2	Model wind turbine . . . . .	14
3.3	Equipment . . . . .	15
3.4	Procedure . . . . .	18
3.5	Scaling and blockage issues . . . . .	19
3.6	Calibration . . . . .	20
3.7	Measurement inaccuracies . . . . .	22
<b>4</b>	<b>Results</b>	<b>24</b>
4.1	$C_P$ , $C_T$ and $M_Z$ . . . . .	26
4.2	Horizontal profiles . . . . .	30
4.3	Velocity contours . . . . .	34
<b>5</b>	<b>Discussion</b>	<b>40</b>
5.1	Performance characteristics and yaw moment . . . . .	40
5.1.1	Power coefficient . . . . .	40
5.1.2	Thrust coefficient . . . . .	41
5.1.3	Yaw moment . . . . .	41
5.1.4	Comparison with calculations using the blade element momentum method . . . . .	43
5.2	Wake measurements . . . . .	44
5.2.1	The effect of tip speed ratio . . . . .	45
5.2.2	Velocity field development . . . . .	45
5.2.3	Yaw angle effect . . . . .	46
5.2.4	Comparison with other results . . . . .	46
<b>6</b>	<b>Conclusion</b>	<b>51</b>
<b>7</b>	<b>Further work</b>	<b>53</b>

<b>A Learning by doing; small wind tunnel measurements</b>	<b>I</b>
A.1 Atmospheric pressure . . . . .	I
A.2 Manometer . . . . .	I
A.3 Day 1, 3/2 - 2011 . . . . .	II
A.4 Day 2, 4/2 - 2011 . . . . .	VI
<b>B Calibration</b>	<b>XII</b>
<b>C Measurement data</b>	<b>XV</b>

## List of Figures

2.1	Forces on the blade geometry of a horizontal axis wind turbine . . .	5
2.2	Airfoil stall . . . . .	6
2.3	Oblique inflow on a wind turbine . . . . .	7
2.4	Blade position . . . . .	8
2.5	The force $F_x$ and the moment caused by this, $M_{Z1}$ . . . . .	9
2.6	The force $F_y$ and the momentum caused by this, $M_{Z2}$ . . . . .	9
2.7	Strømningstube . . . . .	11
2.8	Rotation of the wake behind a wind turbine . . . . .	11
2.9	Streamtube for oblique inflow . . . . .	12
3.1	Closed return subsonic wind tunnel . . . . .	13
3.2	Photo of the wind turbine mounted in the wind tunnel . . . . .	14
3.3	Test turbine dimensions . . . . .	15
3.4	Pitot-static tube . . . . .	16
3.5	Wind tunnel seen from above with the contraction, reference pitot and balance . . . . .	18
3.6	Velocity correlations . . . . .	19
3.7	Calibration of the balance . . . . .	20
3.8	Calibration of the torque . . . . .	21
3.9	Experimental method to find the correct yaw angle . . . . .	22
3.10	Experimental method to place the center of the rotor plane at the center of the balance . . . . .	23
4.1	Power coefficient for different yaw angles . . . . .	26
4.2	Thrust coefficients including contribution from tower and nacelle . .	27
4.3	Thrust coefficients without contribution from tower and nacelle . .	28
4.4	Yaw moment including contribution from tower and nacelle . . . . .	29
4.5	Yaw moment without contribution from tower and nacelle . . . . .	30
4.6	Horizontal velocity profile for $X/D = 1$ . . . . .	31
4.7	Horizontal profiles for different distances behind the rotor plane for $\lambda = 6$ . . . . .	32
4.8	Horizontal profiles for different yaw angles at $X/D = 1$ . . . . .	33
4.9	Horizontal profiles for different yaw angles . . . . .	34
4.10	The velocity field at $X/D = 1$ and $\gamma = 0^0$ . . . . .	35
4.11	The velocity field for $X/D = 1$ and $\lambda = 3$ . . . . .	36
4.12	The velocity field for $X/D = 1$ and $\lambda = 6$ . . . . .	37
4.13	The velocity field for $X/D = 1$ and $\lambda = 9$ . . . . .	38
4.14	The velocity field for $X/D = 4$ and $\lambda = 6$ . . . . .	39

5.1	Total yaw moment calculated using BEM for oblique inflow and $l = 15\%$ of tower height . . . . .	43
5.2	Comparison of data for $X/D = 1, \gamma = 0^0$ . . . . .	48
5.3	Comparison of data for $X/D = 1, \gamma = 30^0$ . . . . .	49
5.4	Comparison of data for $X/D = 4, \gamma = 0^0$ and $\lambda = 6$ . . . . .	50
A.1	Calibrations Day 1 . . . . .	IV
A.2	Vertical velocity profiles for the same velocity day 1 . . . . .	IV
A.3	Calibration Day 2 . . . . .	VI
A.4	Vertical velocity profiles for the same velocity day 2 . . . . .	VII
A.5	Vertical velocity profile day 2 . . . . .	XI
B.1	Calibration of the pressure transducers used for measuring pitot tube pressure, reference pitot pressure at the test section entrance and the contraction pressure(stat) . . . . .	XII
B.2	Torque calibration . . . . .	XIII
B.3	Calibration of the vertical balance cell R1 . . . . .	XIII
C.1	Position of the tower when the turbine is rotated $30^0$ . . . . .	XV
C.2	Vertical profiles for different yaw angles at $X/D = 1$ behind the rotor plane for $TSR = 6$ where a) $\gamma = 0^0$ and $x = 0mm$ , b) $\gamma = 30^0$ and $x = 0mm$ , c) $\gamma = 30^0$ and $x = 67.5mm$ , d) $\gamma = 30^0$ and $x = 80mm$	XVI
C.3	Vertical profiles for different yaw angles at $X/D = 1$ behind the rotor plane for $TSR = 3$ where a) $\gamma = 0^0$ and $x = 0mm$ , b) $\gamma = 30^0$ and $x = 0mm$ , c) $\gamma = 30^0$ and $x = 67.5mm$ . . . . .	XVII
C.4	Vertical profiles for different yaw angles at $X/D = 1$ behind the rotor plane for $TSR = 9$ where a) $\gamma = 0^0$ and $x = 0mm$ , b) $\gamma = 30^0$ and $x = 0mm$ , c) $\gamma = 30^0$ and $x = 67.5mm$ . . . . .	XVIII
C.5	Vertical profiles for different yaw angles at $X/D = 4$ behind the rotor plane for $TSR = 6$ where a) $\gamma = 0^0$ and $x = 0mm$ , b) $\gamma = 30^0$ and $x = 0mm$ , c) $\gamma = 30^0$ and $x = 67.5mm$ . . . . .	XIX

## Nomenclature

$A$	Area [ $m^2$ ]
$c$	Cordlength [ $m$ ]
$C_d$	Dragcoefficient
$C_l$	Liftcoefficient
$C_x$	Axial forcecoefficient
$C_y$	Tangential forcecoefficient
$C_P$	Powercoefficient
$C_T$	Thrustcoefficient
$D$	Rotor diameter
$F_d$	Dragforce [ $N$ ]
$F_l$	Liftforce [ $N$ ]
$F_x$	Axial force [ $N$ ]
$F_y$	Tangential force [ $N$ ]
$l$	Length from rotor plane to tower [ $m$ ]
$m$	Mass [ $kg$ ]
$M_{z1}$	Yaw moment about the tower due to the axial force [ $Nm$ ]
$M_{z2}$	Yaw moment about the tower due to the tangential force [ $Nm$ ]
$M_Z$	Yaw moment [ $Nm$ ]
$\dot{m}$	Massflow [ $kg/s$ ]
$p$	Pressure [ $Pa$ ]
$P$	Power [ $W$ ]
$R, r$	Rotor radius [ $m$ ]
$T$	Thrust force [ $N$ ]
$U$	Wind velocity [ $m/s$ ]
$U_{rel}$	Relative wind velocity [ $m/s$ ]
$X/D$	Distance behind rotor plane
$\alpha$	Angle of attack
$\gamma$	Yaw angle
$\rho$	Density [ $kg/m^3$ ]
$\Omega$	Rotational velocity of the rotor blades [ $\frac{rad}{s}$ ]
$\lambda$	Tip speed ratio
$\varphi$	Angle of incoming relative wind velocity
$\theta$	Blade twist angle
$\psi$	Blade position





# 1 Introduction

In today's society there is a large demand for energy resources. Investment in renewable energy is important to avoid major climate change, and to supply the global energy demand in a sustainable way. This is also the main strategy to reduce emission of damaging greenhouse gases. From the recent events seen in Japan, with the nuclear power plant emissions, it is more important than ever to find other resources to cover the global energy demand. Germany plans to phase out all their nuclear power plants by 2022 and replace the 23% of their energy production, which the power plants are responsible for, with renewable resources.

Wind is a limitless source of pollution free energy. Wind turbines produced today are operating close to their maximum possible efficiency, and large machines are used to make them cost effective. The most common type of wind turbines are the horizontal axis three bladed upwind models. These have a yaw mechanism that turns the nacelle in to the wind every ten minutes due to the unsteady direction of the mean wind.[14] This yaw mechanism wears the structure, and the loads on the construction vary. It also uses electrical power, and makes the top of the turbine heavier than it could be without the yaw mechanism. Downwind turbines have the advantage that they will turn automatically towards the wind and will therefore not need the yaw mechanism. There is not much documented research on the theory of natural yaw on downwind structures.

The wake behind the wind turbine supplies information of the power losses from the machine and turbulence levels that may affect other units. It is important to understand the features of the wake, to decrease the effect the wake from one turbine will have on a construction further downstream. It has been shown that having one wind turbine operating under yawed inflow conditions will increase the power production from the next wind turbine downstream.[1] Therefore it is reasonable to assume that there exist optimal operational conditions for all the single turbines that will give maximal power output from a wind turbine park.

Wind tunnel experiments on the wake behind wind turbines, and the physical loads on the construction are important to perform so that this energy form can be developed further. These experiments have some limitations, for example that the Reynolds number will be lower for test turbines in a closure than for a full scale turbine. This will change the boundary layer development on the blades and result in different turbine characteristics. The power coefficient will have a lower maximum value, but many of the features of the flow will be the same. In a wind tunnel the turbine will have a blockage ratio that will affect the flow, and the rotor plane will work as a porous disc, accelerating the flow locally at the rotor plane.[11]

The aim of this thesis is to learn the experimental techniques required to measure

forces and moments on a model turbine, as well as measuring the mean velocity in the flow. With the model turbine mounted in the tunnel, the forces and moments are to be measured as a function of the yaw angle for both upstream and downstream configuration. The growth rate and path of the wake are to be determined for some selected turbine operating conditions.

A review of wind turbine theory is first outlined, and then follows the experimental setup and techniques required for wind tunnel experiments. The results are displayed graphically and compared with previous calculations using the blade element momentum method for oblique inflow, and measurements performed by Adaramola [2].

## 2 Theory

### 2.1 Wind turbine physics

Wind turbines are constructed to extract as much kinetic energy from the wind as possible. The most common wind turbines used today are the horizontal axis wind turbines (HAWTs). The blades are mounted on the hub parallel to the tower (unless they have a coning angle) and these are again perpendicular to the nacelle. There are two different configurations for the wind turbine. It is either upwind or downwind. The difference between the two are that for the upwind turbine the rotor is upstream from the tower, and for the downwind the blades are downstream from the tower. It is expected that a downwind turbine can operate with free yaw, and self rotate in to the wind direction, compared to the upwind turbine that usually has a yaw mechanism installed. [15] Complexity, downtime and maintenance costs can be reduced by this passive free yawing solution. Still, the system yaw rotation may be unstable at some operating conditions, and also a constant free yawing in one direction can be problematic for electrical setup.[17] Downwind turbines can also have an advantage in complex terrain (hills and mountains) due to the wind direction changes. The upstream wind turbine is still the most common configuration used, much because the marked for the wind turbines initially was developed in areas of flat terrain. [18]

#### 2.1.1 Forces and moments on a wind turbine

A wind turbine in operation experience aerodynamic forces caused by the wind, see figure 2.1. The available energy in the wind for a given cross section normal to the wind direction is  $P = \frac{1}{2}\rho U_{\infty}^2 A$ .

The lift force on a wind turbine blade is defined to be perpendicular to the incoming wind,  $U_{rel}$  in figure 2.1. This force is a consequence of the pressure difference on the upper and lower side of the airfoil.

$$dF_l = \frac{1}{2}\rho C_l(\alpha) c U_{rel}^2 dr \quad (2.1)$$

The drag force is defined to be parallel to the incoming flow  $U_{rel}$ . The cause of this force is both viscous friction at the surface and unequal pressure on the airfoil surfaces facing away from and towards the incoming flow. [15]

$$dF_d = \frac{1}{2}\rho C_d(\alpha) c U_{rel}^2 dr \quad (2.2)$$

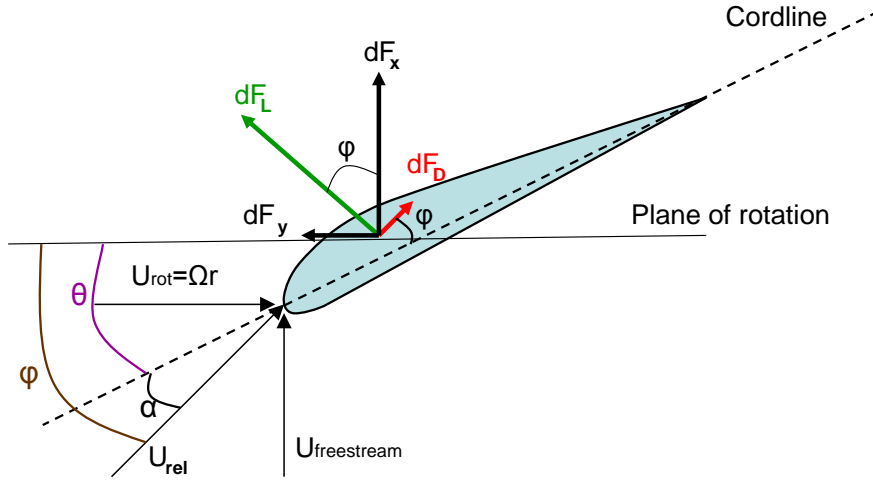


Figure 2.1: Forces on the blade geometry of a horizontal axis wind turbine

The lift and drag coefficients,  $C_l$  and  $C_d$ , are dependent on the angle of attack and are known for a given blade profile. Torque and thrust forces a wind turbine experience are dependent on the lift and drag forces. A simplified explanation of these components is that the lift force contribute to increasing the power production while the drag force have the opposite effect.

### Tip speed ratio

The tip speed ratio,  $\lambda$ , is defined as the ratio between the blade tip speed and the wind velocity.

$$\lambda = \frac{\text{Bladetipspeed}}{\text{Windspeed}} = \frac{\Omega R}{U_\infty} \quad (2.3)$$

Omega,  $\Omega$ , is the angular velocity of the rotor,  $R$  is the rotor radius and  $U_\infty$  is the freestream velocity.

Stall can often occur when the tip speed ratio,  $\lambda$ , is low. This is due to the high angle of attack,  $\alpha$ , each blade element experience at low  $\lambda$ . Surface friction will slow the flow next to the airfoil surface due to the viscosity of the air. This results in a separation of the boundary layer on the upper surface of the airfoil and a wake forms above the blade which reduce lift and increase drag, see figure 2.2. Stalling starts at the root of the blade where  $\alpha$  is high. This effect is sometimes used to limit the wind turbine power in high winds, and a well designed stalling system has a nearly constant output even though the wind speed changes. [15]

When the tip speed ratio is high, the inner part of the wind turbine blade can

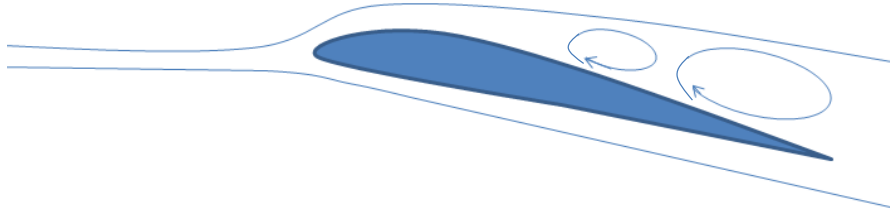


Figure 2.2: Airfoil stall

experience negative angle of attack. This will result in the blade working as a propeller and transferring power to the wind instead of extracting it. This can give a higher velocity in parts of the wake compared to the freestream velocity.

### Power and thrust coefficient

The blades on a wind turbine are rotating due to the incoming wind. This creates a torque on the horizontal axis which is converted to electrical energy by the use of a generator. It is impossible to extract all the available power from the wind. Limitations in the physics behind the turbine as well as mechanical losses contribute to lowering the efficiency. A parameter that explains how well a wind turbine can extract power from the wind is the power coefficient,  $C_P$ . This is defined as the ratio between produced and available power.

$$C_P = \frac{\text{Rotor power}}{\text{Power in the wind}} = \frac{P}{\frac{1}{2}\rho U_\infty^3 A} \quad (2.4)$$

Modern wind turbines have a power coefficient of around 50%. This is close to the maximum  $C_P$  that a wind turbine can achieve:  $C_{Pmax} = \frac{16}{27} = 59,26\%$ . This is known as the Betz limit. [15, page 87-88]

In addition to the torque created by the wind, there is also a force in the streamwise direction induced by the pressure drop over the rotor. This causes fatigue loads on the turbine, and therefore the construction must be built so it can withstand these forces. The thrust coefficient is defined as the relation between the thrust force on the turbine and the dynamic force in the wind.

$$C_T = \frac{\text{Thrust force}}{\text{Dynamic force}} = \frac{T}{\frac{1}{2}\rho U_\infty^2 A} \quad (2.5)$$

### 2.1.2 Yaw angle

A real turbine in operation will not always experience wind perpendicular to the rotor plane. In periods of the production time, the incoming wind will be oblique as shown in figure 2.3.

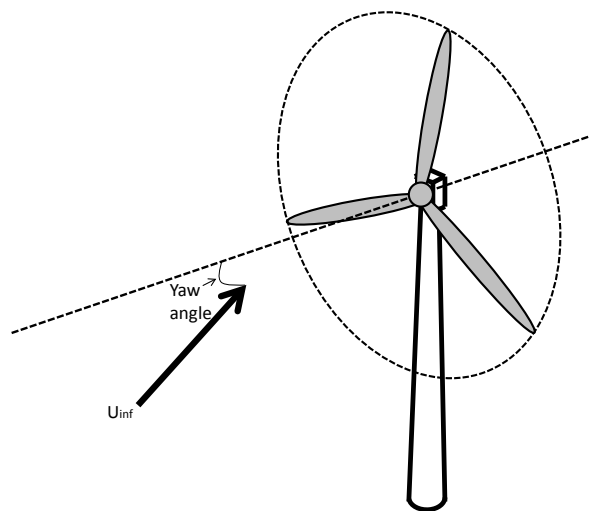


Figure 2.3: Oblique inflow on a wind turbine

A positive yaw angle is defined to be in the clockwise direction.

Because of the oblique inflow, the wind turbine blades will experience other dynamical loads than those already described. The wind turbine blades will move partially in and out of the wake and the incoming flow. This causes the relative wind velocity every element of the blade experience,  $U_{rel}$ , to change with position of the blade,  $\psi$ . Definition of the wind turbine blade position is shown in figure 2.4.

When the rotor plane on a turbine is not perpendicular to the wind, the efficiency will decrease. Therefore most modern wind turbines today have a yaw system which rotates the rotor plane in to the wind. If this yaw system is very sensible and constantly rotate the rotor plane perpendicular to the incoming wind, the mechanical components will experience reduced lifetime due to the constant motion. Therefore this is a matter that must be carefully considered and developed. [9, page 362]

There are conflicting aims when it comes to the matter of controlling wind turbine yaw motion. Since the efficiency decrease for a wind turbine with the rotorplane oblique to the incoming flow, one should think that the optimum situation in a wind park would be having all the rotor planes perpendicular to the incoming wind

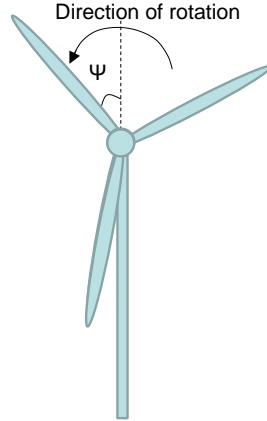


Figure 2.4: Blade position

direction. This is not necessarily the case. In some situations, the reduced power output from one unit due to deviation from the incoming flow, can give increased power output from a unit downstream of the first. It is therefore reasonable to assume that there can be a combination of yaw angle and maximum power output from a wind farm.[9, page 362] This matter will not be discussed further in this thesis, but for more information on this subject see Krogstad and Adaramola [1].

There are two different forces that are the origin for the natural yaw moment on a wind turbine oblique to the incoming flow. These are the forces  $F_x$  and  $F_y$  shown in figure 2.1. When the rotorplane is perpendicular to the incoming flow,  $F_x$  and  $F_y$  will be symmetrical about the vertical and horizontal line that crosses the center of the rotorplane respectively. When the incoming flow is oblique, this is no longer the case. The turbine will then experience a natural yaw moment that will try to turn the rotor in to or out of the wind. A positive yaw moment tries to rotate the construction in the clockwise direction. The yaw moment for a downstream wind turbine with the rated power of  $140kW$  can be in the order of  $4000Nm$ . [17]

The force  $F_x$  will act on the distance from the tower and to the blade element where it has its origin. This will cause the moment  $M_{z1}$ . The arm will be horizontal and follow the blade in to the center of the rotor. If the rotorplane is divided in a vertical line through the center, the side where the total  $F_x$  is largest will be determining for the direction of the rotation  $M_{z1}$  causes. See figure 2.5.

The position of the blade,  $\psi$ , will be of importance for the quantity of the moment since the force  $F_x$  vary with position, see equation (2.6).

$$M_{z1} = F_x r \cos \psi \quad (2.6)$$

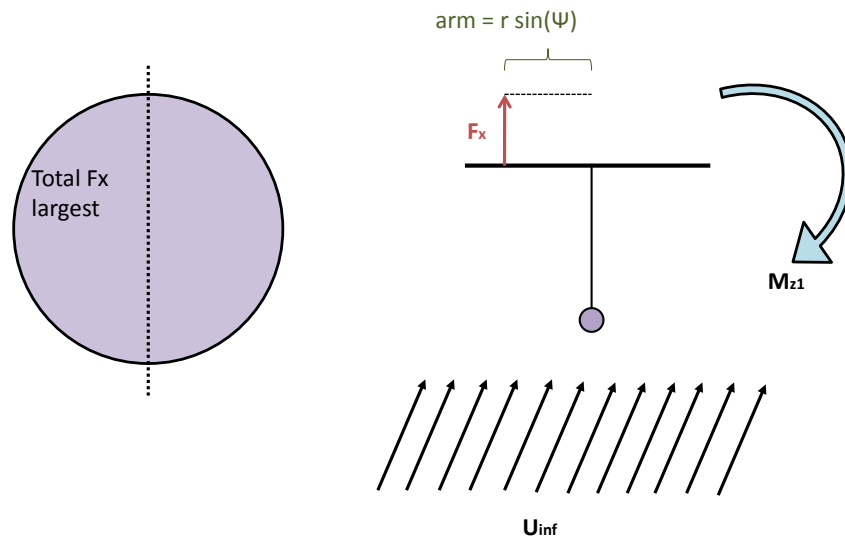


Figure 2.5: The force  $F_x$  and the moment caused by this,  $M_{Z1}$

$F_y$  is in its entirety determining for the power production. The horizontal part of this force will also be the origin of a yaw moment about the tower axis,  $M_{Z2}$ . The distance from the tower and in to the rotor plane will be the arm in this moment. If the rotor plane is divided with a horizontal line through the center, the part where the total  $F_y$  is largest will be determining for the rotational direction caused by  $M_{Z2}$ . See figure 2.6.

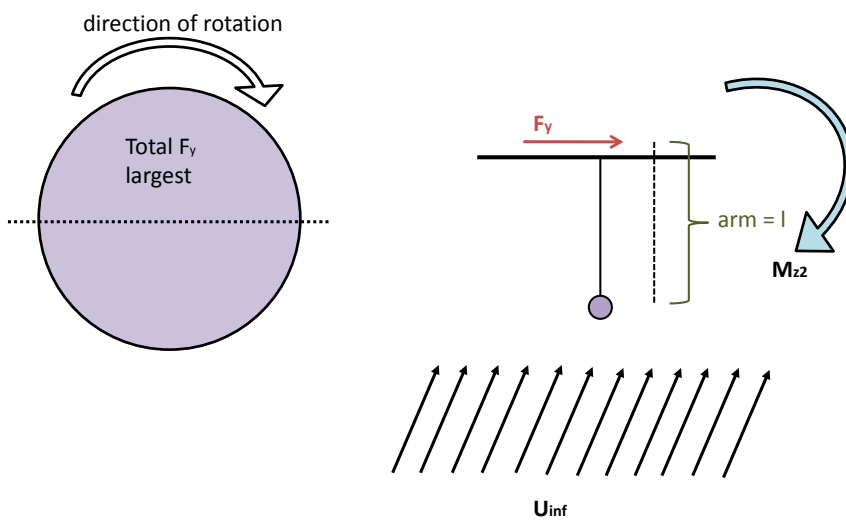


Figure 2.6: The force  $F_y$  and the momentum caused by this,  $M_{Z2}$



Since the force  $F_y$  is no longer symmetrical when the inflow is oblique,  $M_{z2}$  will also be dependent on the blade position.

$$M_{z2} = F_y l \sin \psi \quad (2.7)$$

## 2.2 Wind turbine wakes

After three diameters downstream of the rotor plane, much of the periodic nature in the flow is lost and the tip vortices diffuse. This is what is known as the near wake area, and is usually described as two to four diameters length from the rotor plane. After the near wake is the far wake, where turbulence and velocity profiles are more evenly distributed due to diffusion of turbulence and vorticity generated at the rotor. [15]

Turbines downwind of other units will experience higher turbulence levels due to producing upwind machines. This increased turbulence results in larger loads and material fatigue which reduce turbine lifetime. The energy capture is also reduced because of the increased turbulence levels for downstream units, but the steady state load is reduced due to the lower mean velocity of the flow.[9, page 117]

### 2.2.1 Wake expansion

A wind turbine extract kinetic energy from the wind, and therefore reduce the mean velocity of the flow passing through the rotor. Assuming that the mass affected is completely separated from the surrounding air and does not experience any boundary effects, a stream tube can be constructed which illustrate the air passing a wind turbine, see figure 2.7. As the air passes through the rotor, both velocity and static pressure is reduced. Since the air is not compressed and the mass flow rate in the stream tube remains the same, the cross-sectional area of the streamtube must expand due to the lower air velocity. The part of the streamtube in figure 2.7 that continues downstream from the rotor is what is known as the wake. [4, page 42]

As the wake extends downstream of the rotor, the centerline velocity deficit decrease, and the width increase.[3] The growth rate,  $\frac{dr}{dx}$ , can be used to describe how much the wake expands when moving downstream. [5] When the thrust coefficient increase, the expansion of the wake increase.

Low velocities will cause a large jump in velocity from  $U_1$  to  $U_4$  in figure 2.7. This will again result in a turbulent-wake state, which is formation of eddies that brings momentum in to the wake from the outer flow. [8]

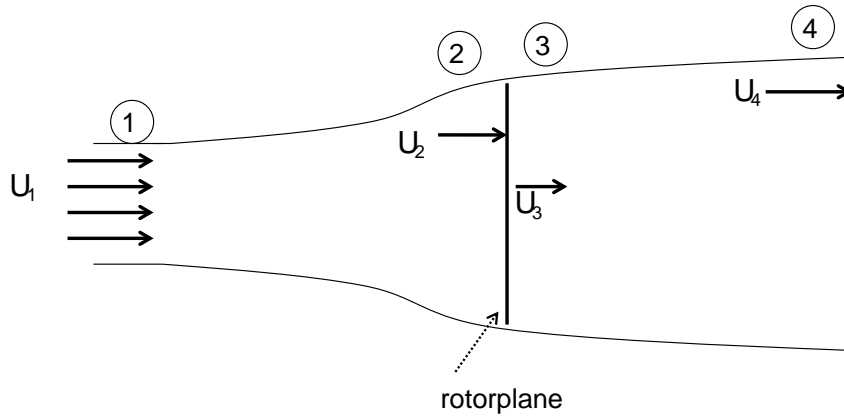


Figure 2.7: Strømningsstube

The rotor thrust coefficient has a large influence on the extent of the wake due to the significant influence on the loss of impulse behind the rotor. The wake behind the rotor is also dependent on the turbine operating conditions, as for instance the tip speed ratio, blade pitch angle etc.

### 2.2.2 Wake rotation

When air is passing the rotor disc it experience a torque. This is the origin for the power production and rotation of the blades. An equal and opposite torque is required due to Newton's third law, and this causes the wake to rotate in the opposite direction to that of the rotor. Due to the wake rotation there will be a tangential velocity component which increase the kinetic energy in the wake. This is compensated for by a drop in the static pressure of the air in addition to the reduction in static pressure when the wind passes through the rotor.[4]

Wake rotation in a streamtube is illustrated in figure 2.8.

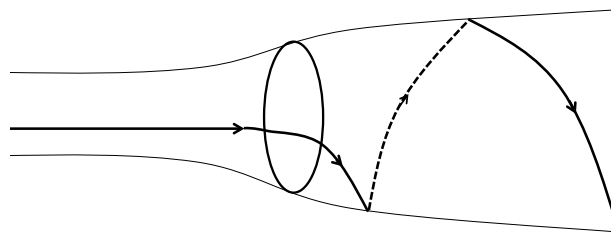


Figure 2.8: Rotation of the wake behind a wind turbine

### 2.2.3 Wake with yaw angle

The rotor acts like a disc seen from a global perspective, and when the incoming wind is not perpendicular to the rotor plane there will be a discontinuity in the pressure drop across the disc. The pressure drop generates the thrust which again induce a velocity normal to the rotor plane that deflects the wake as shown in figure 2.9.[8, page 90-91] Hence it follows that when the rotor plane is not perpendicular to the incoming wind flow, the wake will be asymmetric. This results in the downwind part of the rotor being closer to the wake centerline, and experience higher induced velocities and forces. [15]

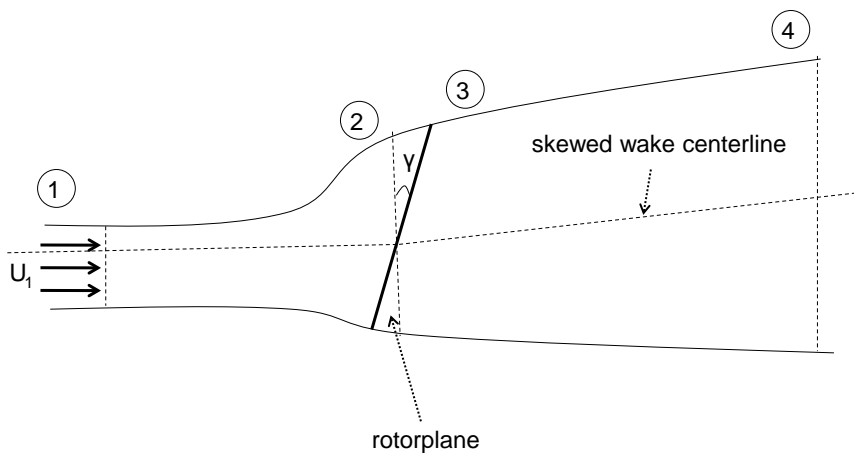


Figure 2.9: Streamtube for oblique inflow

## 3 Experimental setup

### 3.1 Wind tunnel

The experiments performed in this thesis were conducted in the closed return low speed wind tunnel at the Department of Energy and Process engineering at The Norwegian University of Science and Technology, see figure 3.1. The test section has a height of 2 meters, width = 2.7 meters and length = 9 meters. The height of the test section increases from the inlet of the tunnel to approximately 2.3 meters at the outlet so that the streamwise pressure gradient is zero and the wall boundary layer growth is accounted for.



Figure 3.1: Closed return subsonic wind tunnel

The fan installed is 220 kW and is able to provide velocities of up to 30 m/s within the test section. At constant conditions the streamwise centerline velocity can vary with 0.5%. [7]

The turbine is placed on a six component force balance which allows measurement of forces in three dimensions. The software ForceLog is used to measure the forces and directly gives the yaw moment which is of interest in this thesis. The scale can be rotated 360 degrees with respect to the tunnel axis, which enables measurements at different yaw angles.

In the tunnel there is installed a three-axis traversing system which is controlled

by a computer. This allows flow measurements at all the positions needed in this thesis.

### 3.2 Model wind turbine

The wind turbine used in the experiments is a horizontal axis wind turbine with a three bladed upwind rotor and diameter of 900mm. The height from the floor of the test section to the center of the hub is measured to be 817mm.

The wind turbine placed in the wind tunnel is displayed in figure 3.2.

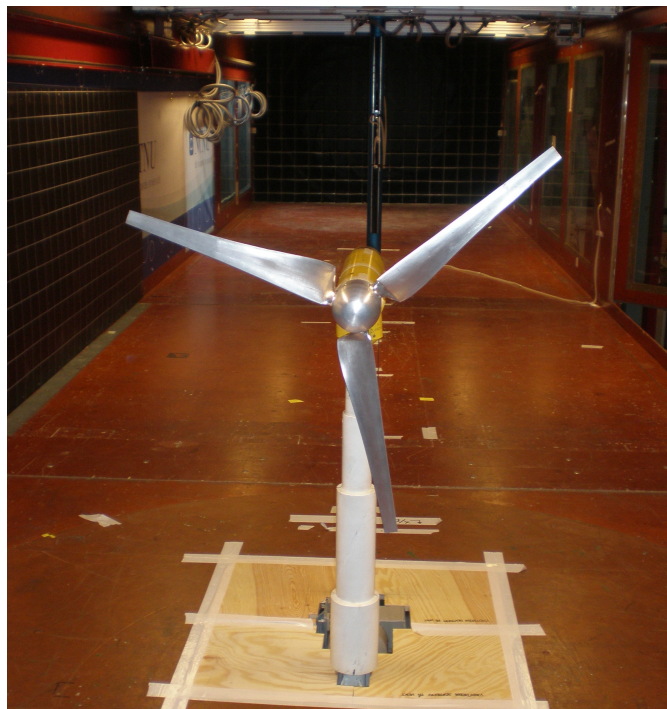


Figure 3.2: Photo of the wind turbine mounted in the wind tunnel

Blade geometry is developed by Per-Åge Krogstad and Jon Amund Karlsen [12]. The blades are constructed so that they will have the same properties as a large operating machine when placed in the wind tunnel. The main difference between the test turbine and a real operating turbine is the Reynolds number. A real turbine experience  $Re$  of approximately  $2 \cdot 10^6$ , but the test turbine will have a Reynolds number approximately 20 times lower than this. The design was corrected for the expected Reynolds number effect on the airfoil characteristics. More information on the wind turbine blades can be found in Krogstad and Karlsen [12].

The rotor was controlled by an asynchronous motor where the rotational velocity of the blades could be set. At the back of the hub, a transmission belt was

connected to a generator beneath the floor of the wind tunnel. This generator was again connected to the asynchronous motor which allowed the controlling of the rotational speed of the turbine blades.

The tower has an increasing perimeter from the top and down with three different circumferential lengths which can be seen in figure 3.3. A circular cylinder is used as the hub, and in this casing the thrust gauge is placed.

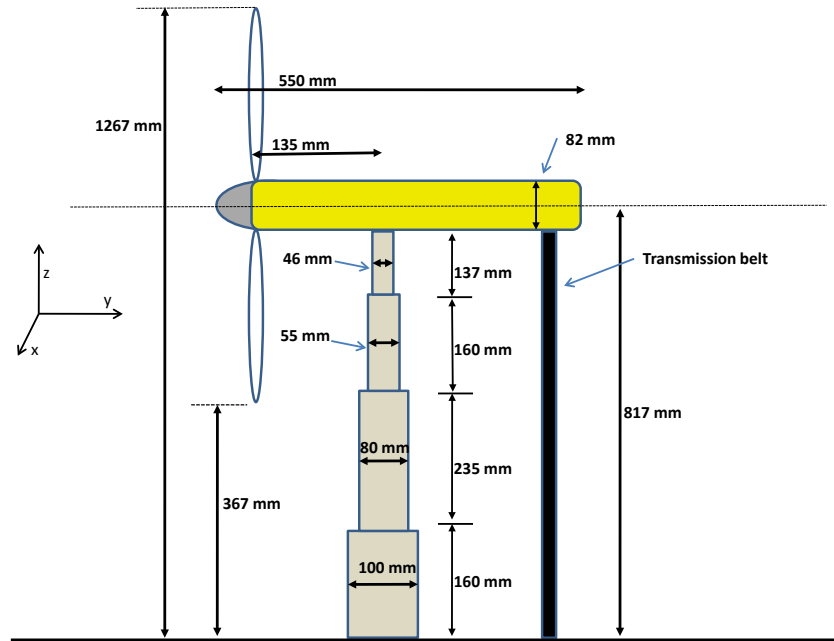


Figure 3.3: Test turbine dimensions

During the tests the rotor rotates in an anticlockwise direction when seen from upstream. The blades were rotated  $180^{\circ}$ , and so was the turbine, for the downwind turbine setup. Therefore the rotational direction was the same for both upstream and downstream configuration.

### 3.3 Equipment

#### Pitot-static tube

A pitot-static tube (Prandtl tube) is used to measure the mean velocity in the flow. There is a center hole down the axis of the tube which is pointed in the direction of the flow and measure the total pressure,  $p_{tot}$ . On the outside of the tube there are small holes perpendicular to the one in the center, and these measure the stagnation pressure  $p_s$ . A pressure transducer measure the strain in a thin

element using an electronic strain gauge, and is used to find the difference between  $p_{tot}$  and  $p_S$ . This equals the dynamic pressure,  $p_{dyn}$ , as can be seen in equation (3.1).

$$p_{dyn} = p_{tot} - p_S \quad (3.1)$$

Knowing the air density and dynamic pressure, the mean velocity in the flow can be found from Bernoulli's equation:

$$p_S + \frac{1}{2}\rho U^2 = p_{tot} \quad (3.2)$$

and this gives the following expression for the velocity

$$U = \sqrt{\frac{2(p_{tot} - p_S)}{\rho}} \quad (3.3)$$

An illustration of how the pitot-static tube is constructed can be seen in figure 3.4.

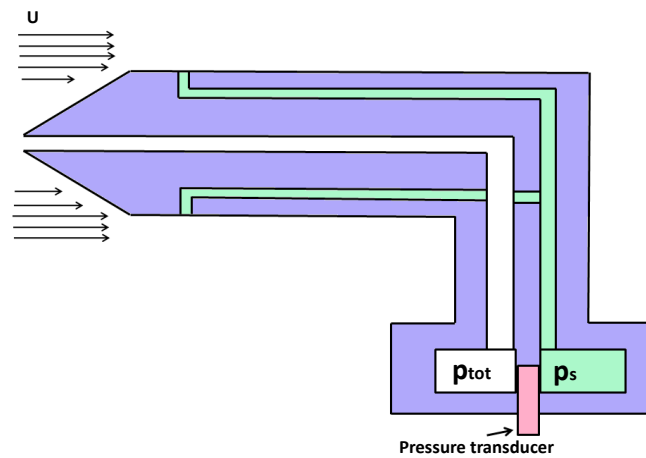


Figure 3.4: Pitot-static tube

### Contraction

At the inlet of the test section there is a contraction of the tunnel area. Equipment is installed for measuring the static and total pressure at two different positions in this contraction. To calculate the mean velocity in the flow, the reduction in area from the first position to the second must be accounted for. This can be done by applying the conservation of mass:

$$U_1 A_1 = U_2 A_2 \quad (3.4)$$

$$U_1 = \frac{A_2}{A_1} U_2 \quad (3.5)$$

where  $1 - \left(\frac{A_2}{A_1}\right)^2 = 0.967$  for this tunnel. From the Bernoulli equation the velocity can then be expressed:

$$\frac{1}{2}\rho U_1^2 + p_1 = \frac{1}{2}\rho U_2^2 + p_2 \quad (3.6)$$

Combining equation (3.5) and (3.6) gives the expression for the velocity at the inlet:

$$U_2 = \sqrt{\frac{2\Delta p}{\rho \left(1 - \left(\frac{A_2}{A_1}\right)^2\right)}} \quad (3.7)$$

The pressure transducer is also used in this case to measure the pressure difference.

### **Manometer**

A manometer is a simple construction which contains methylated spirit. When measurements are done, this is connected to the pitot tube. The pressure in the airflow increase, and the methylated spirit pillar increase. In this way it is possible to calculate the pressure in the flow from  $P = \rho g h_{MethSp}$ . The instruments is used in the calibration process, and the pressures calculated from the height of the methylated spirit pillar has a linear correlation with the voltage registered when varying the velocity in the test section.

### **Amplifier**

This instrument is used to amplify the signal from the pressure transducer so that more accurate measurements are possible.

### **Pressure transducer**

The pressure transducer converts the measured pressure in to an analog electrical signal which is logged by the software GenLog. Through the procedure of calibration of the pressure transducer, a constant that correlate voltage and pressure is obtained. It is then possible to find the real pressure at a wanted position in the flow from the calibration constant and the measured voltage.



### 3.4 Procedure

#### Velocity correlation

When the wind turbine is placed in the test section it is not possible to measure the flow velocity at hub height. Placement of a pitot-tube in front of the turbine would disturb the flow. Therefore it is necessary to use the contraction or the reference pitot (see figure 3.5) to calculate the freestream velocity seen by the construction. This is done by placing the pitot where the hub-center of the turbine will be placed. Then the velocity in the tunnel is varied and measured at the three different positions; contraction, reference pitot-tube and pitot tube at hub position.

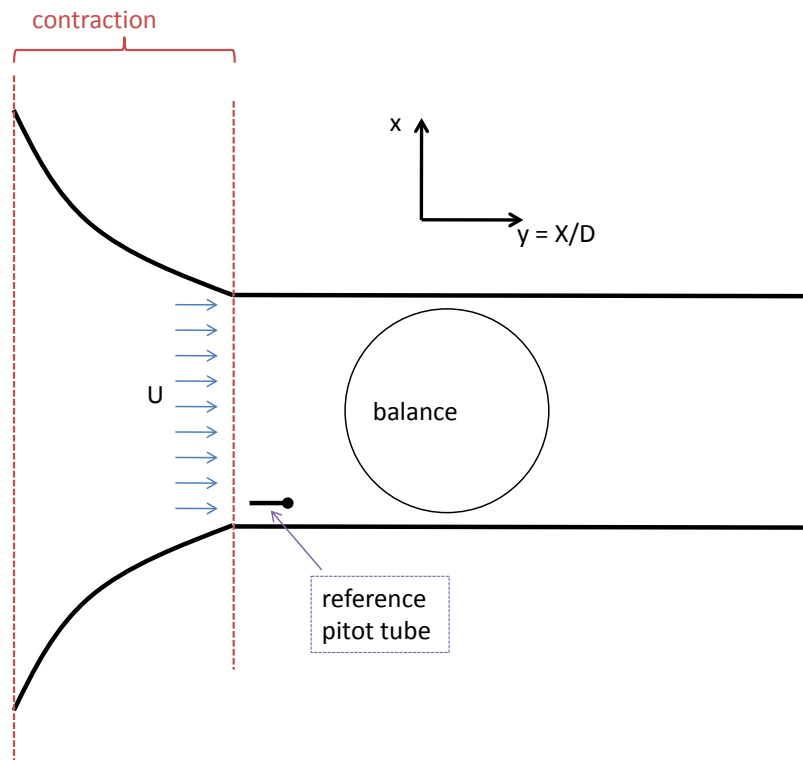
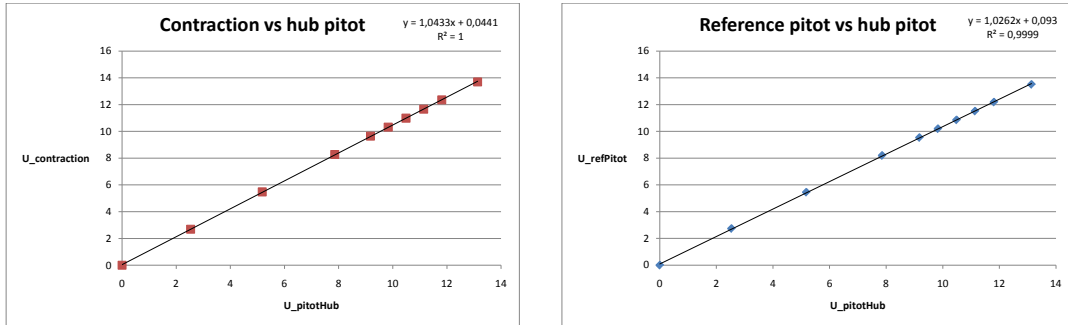


Figure 3.5: Wind tunnel seen from above with the contraction, reference pitot and balance

From figure 3.5 it can be seen that the length of the tunnel,  $y$ , is described as  $X/D$  where  $D$  is the rotor diameter. This is a suitable parameter to use in this thesis, since it is common to describe the distance behind the rotor plane in diameters of the rotor.

A graph is then constructed which shows the correlation between the contraction and the pitot at hub position velocity, and also one for the correlation between the

reference pitot and the pitot at hub position. See figure 3.6.



(a) Contraction vs Hub pitot

(b) Reference pitot vs Hub pitot

Figure 3.6: Velocity correlations

When the turbine is mounted in the tunnel, the correlations in figure 3.6 are used to calculate the freestream velocity experienced by the turbine. It is assumed that the change in the contraction velocity and the reference pitot velocity is the same as the change in the velocity at hub height when the turbine is placed in the test section. The velocity correlations is therefore used to calculate the freestream velocity seen by the turbine.

As can be seen, the reference pitot and the contraction does not give the same correlation. Only one of these velocity references should be used in the measurements. This is explained further in section 4, Results.

### 3.5 Scaling and blockage issues

When doing measurements in a wind tunnel there are two effects that can reduce the validity of the tests. These are the scaling issues and the interference from the walls, also called the blockage effect.

The blockage ratio is defined to be the ratio between the rotor swept area and the wind tunnel cross sectional area. The suggested upper limit for this blockage ratio is 10% to avoid wind tunnel wall interference on the measurements [1]. If the wake can expand freely, the blockage effect can be neglected[6].

The rotorswept area in this case is  $\pi r^2 = \pi(0.45m)^2 = 0.647m^2$  and the cross sectional area of the tunnel is  $width \cdot height = 1.9m \cdot 2.7m = 5.1m^2$ . This gives a blockage ratio of  $\frac{0.64m^2}{5.1m^2} = 12\%$  which is close to the suggested upper limit of 10%.

The ratio between the tower height and the rotor diameter,  $\frac{835.7}{450} = 1.86$ , is similar to that of full scale turbines. Therefore the floor interference on the flow is assumed to be similar to the ground interference on full scale turbines. The side walls are symmetric and can be compared with turbines placed on the sides of the test turbine as in a wind park.. The test section is 1.9m high, and the roof is therefore located  $1900\text{mm} - 817\text{mm} = 1083\text{mm}$  above the center of the rotorplane. This places the roof approximately  $1.2D$  above the nacelle, and one can therefore expect some interference from the roof on the final results.

### 3.6 Calibration

The experiments in this thesis were not all completed at the same time. For each period measurements were conducted it was necessary to calibrate the equipment that were to be used.

#### Balance

The balance has six sensors that has to be calibrated. By applying different known amounts of mass to each of these sensors and registrate the voltage, it is possible to find the calibration constants by linear regression. The unit of the calibration constant for the balance sensors is  $[\frac{N}{V}]$ . An example of the calibration curve for the balance can be found in Appendix B.

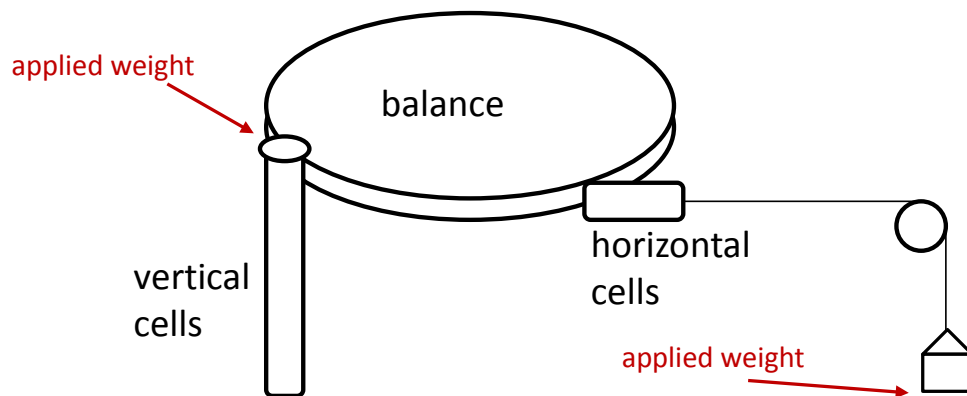


Figure 3.7: Calibration of the balance

#### Torque

The torque is calibrated using weights in the range 0g to 400g. The setup for the calibration can be seen in figure 3.8. The voltage obtained from the measurements when increasing the weight on the blade is plotted against the moment calculated

from  $M[\text{kg}] \cdot g \cdot \text{arm}$ . From this the calibration constant can be found, and this has the unit  $[\frac{\text{Nm}}{\text{V}}]$ . The calibration curve for the torque can be found in Appendix B.

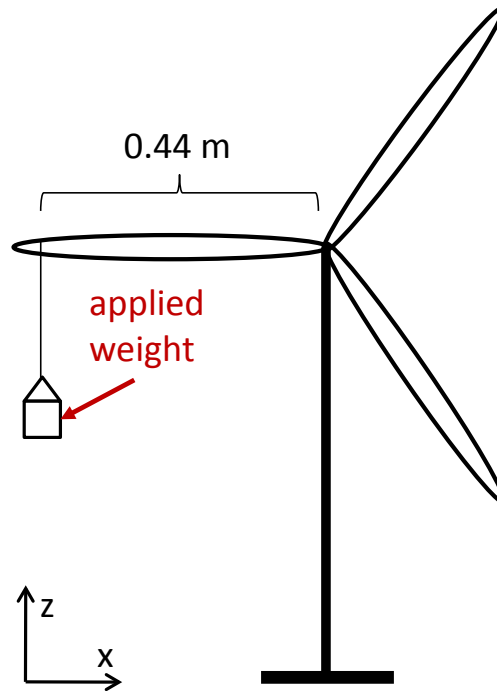


Figure 3.8: Calibration of the torque

### Pressure transducers

The reference pitot tube, contraction and the pitot tube used for wake measurements were connected to a manometer, pressure transducer and amplifier. By using the software GenLog the voltage was logged for each measurement.

When increasing the rotational velocity of the fan in the wind tunnel, it is expected that the voltage measured at the different positions and the pressure calculated by use of the manometer has a linear correlation. From this it is possible to find a calibration constant for each of the amplifiers used so that the pressure at a wanted position can be found from the measurement in volts. The unit of the calibration constant is  $[\frac{\text{Pa}}{\text{V}}]$ . One example of the calibration curve for the pressure transducers can be found in Appendix B.

### 3.7 Measurement inaccuracies

When the velocity field behind the wind turbine was measured, the balance was rotated manually to obtain a yaw angle of  $30^0$ . This was done by measuring the distance from the rotor plane to the edge of the balance. Then the balance was rotated, and a new distance perpendicular to the rotor plane and to the edge of the balance was marked. The distance between these two points at the edge of the balance,  $L$ , was then measured. When the distance  $L$  that gave the correct yaw angle of  $30^0$  was found, the balance was locked in position. See figure 3.9.

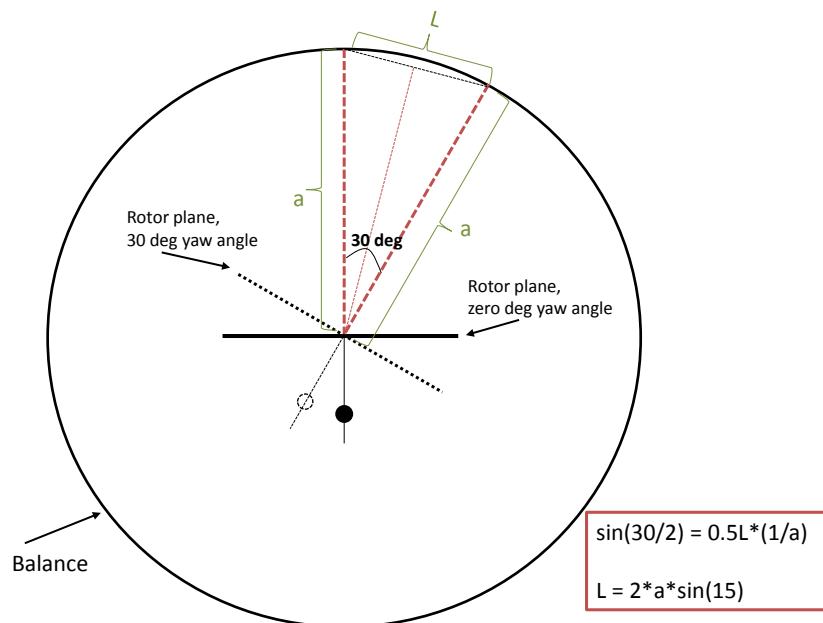


Figure 3.9: Experimental method to find the correct yaw angle

This method contains several inaccuracies, for example that the yaw angle was not exactly  $30^0$ .

There was no reference for placing the wind turbine at a yaw angle of zero degrees with the rotor plane in the center. This was done by eye measurement, and therefore it is probable that the rotor plane was not completely perpendicular to the wind. Since the experiments were not performed during the same time period, the angles might have different inaccuracy values since the turbine position probably varied each time it was set up.

When the rotor was placed at the center of the hub, this was also done approximately. A cotton thread with a nut in the end was fastened to the roof above the center of the balance. Then the turbine was placed so that the nut was at the center of the rotor plane. See figure 3.10.



Figure 3.10: Experimental method to place the center of the rotor plane at the center of the balance

Before measurements were carried out, the amplifier, pressure cells on the balance and other equipment was found to be without serious inaccuracies. Still, there can have been some inconsistency in the instruments that was not measurable. The manual readings of the mercury and methylated spirit for the atmospheric pressure and pressure in the flow, respectively, was not 100% accurate. The error related to these readings is expected to be negligible.

## 4 Results

Different operation conditions and distances behind the rotor plane has been measured for the velocity field. The different cases and combinations of operating conditions can be seen in table 4.1.

Table 4.1: The different cases examined for the wake

TSR	3	6	9
Yaw angle	0 and 30	0 and 30	0 and 30
X/D	1	1, 4 and 7	1

The yaw moment, power coefficient and thrust coefficient curves has also been examined. This has been done for  $TSR = 3, 6$  and  $9$  and for the yaw angles  $\gamma = 0^\circ, 10^\circ, 20^\circ$  and  $30^\circ$ .

The center of the rotor plane is defined as  $[x, z] = [0, 0]$ .

Two different methods of calculating the velocity at the hub of the wind turbine has been described in the section 3.4. These two methods does not give the same answer, therefore one of them must be chosen. It is assumed that the reference pitot tube does not participate in the streamtube that can be seen in figure 2.7. Therefore it is not certain that the measurements at this point will correlate with the changes at the hub when the wind turbine is mounted in the tunnel. The contraction will give the mean velocity of the entire section, see figure 3.5. This solution will also have a limited accuracy, since only parts of the contraction participate in the streamtube. Still, it will be more accurate than using the reference pitot. In the results calculated, the contraction correlation is therefore used when obtaining the hub velocity.

For all the horizontal profiles and velocity field measurements, the velocity has been normalized with the freestream velocity,  $U_{hub}$ . The distances in  $x$  and  $z$  direction has been normalized with the radius  $r$ , and the length of the tunnel, the  $y$  direction, is described as  $X/D$ .

The velocity field measurements were first performed with a grid that had the distance  $15cm$  between each point measured both in height and width and a total number of 81 measurement points. This was found to be too coarse, so the grid size was decreased with  $10cm$  in each direction, and the distance between the points was set to be  $10cm$ . The grid consists of 143 points for the measurements where  $X/D = 1$ , and 169 points for  $X/D = 4$  since it was expected that the wake would expand.

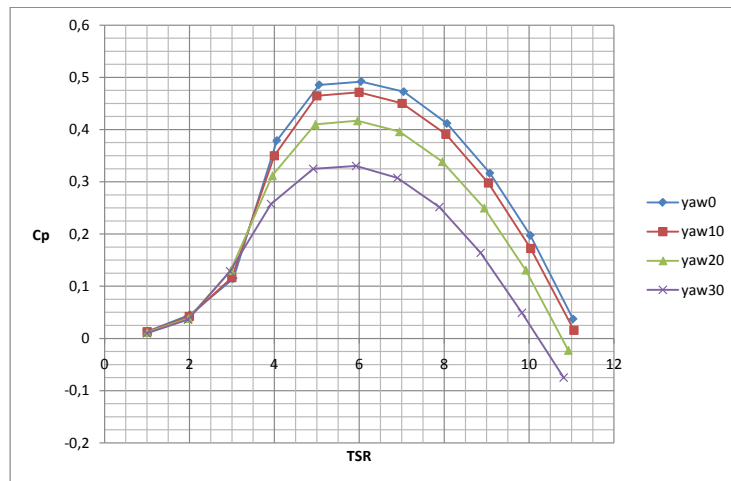
The measurement frequency was  $400\text{Hz}$  and 12000 samples, which gave a sampling time of 30 seconds. The rotational velocity of the wind turbine blades was measured using a tachometer. The results from using this was compared to the use of an oscilloscope. They were found to be very similar, but the oscilloscope was more difficult to read so the RPM of the turbine was based on the Tachometer measurements.

For the  $C_P$ ,  $C_T$  and  $M_Z$  measurements there had been installed a logging system for the RPM of the rotor blades. This was found to vary with 0.5% to 2% compared to the tachometer. This logging was therefore used for these measurements since the tachometer requires entering the wind tunnel and is more time consuming. The tachometer alone could also give a variation in the rotational velocity of about  $10\text{rpm}$ .

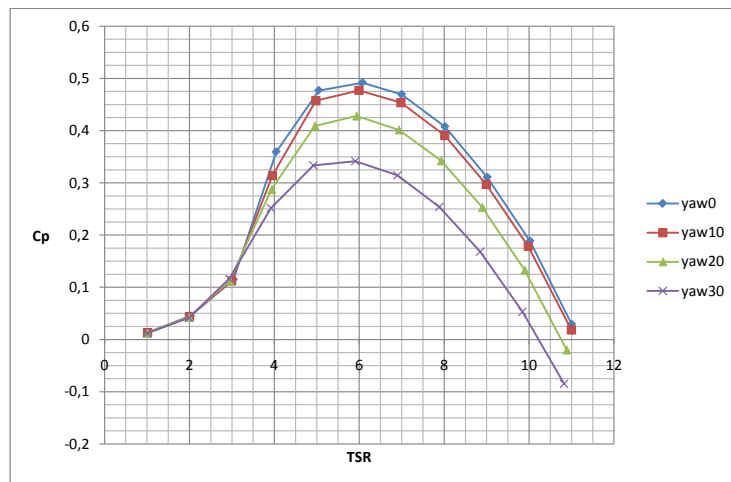


## 4.1 $C_P$ , $C_T$ and $M_Z$

Power coefficient,  $C_P$ , thrust coefficient,  $C_T$ , and yaw moment,  $M_Z$ , has as mentioned been measured for  $\gamma = 0^\circ, 10^\circ, 20^\circ$  and  $30^\circ$ . This has been done for both upstream and downstream configuration. When the turbine is used as a downwind machine, the blades and construction are rotated  $180^\circ$ , so the same set of blades have been used in all the measurements.



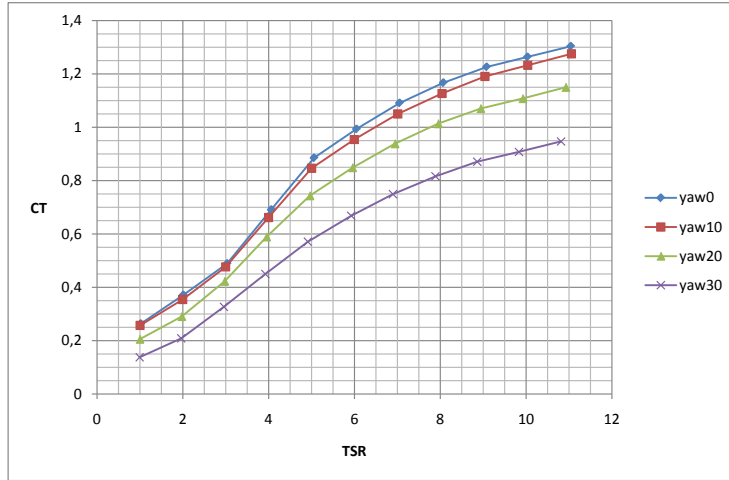
(a) Upstream configuration



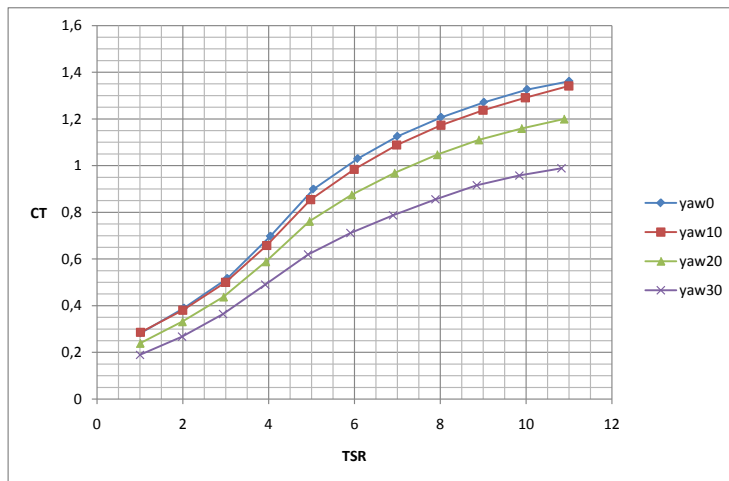
(b) Downstream configuration

Figure 4.1: Power coefficient for different yaw angles

The power coefficients for various yaw angles and tip speed ratios are shown in figure 4.1 for both upstream, 4.1a, and downstream, 4.1b, configuration.



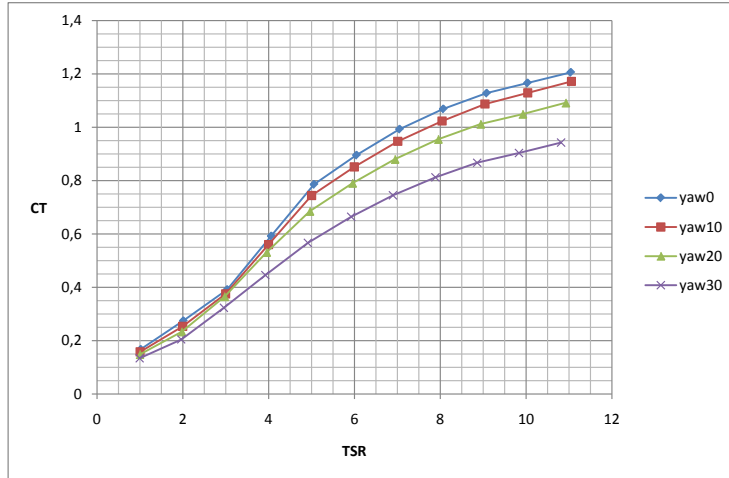
(a)  $C_T$  for upstream configuration



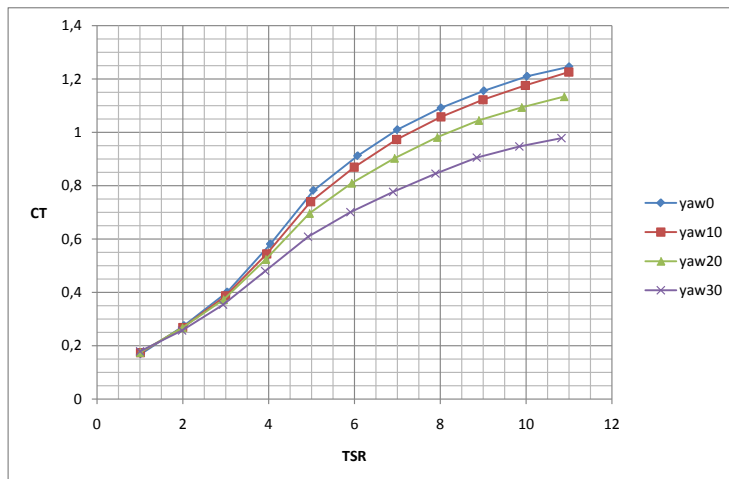
(b)  $C_T$  for downstream configuration

Figure 4.2: Thrust coefficients including contribution from tower and nacelle

The thrust coefficients for different yaw angles for the entire construction are shown in figures 4.2a and 4.2b for upstream and downstream configuration respectively. After subtracting the effects from the tower and nacelle, the thrust coefficients are plotted again. These graphs are plotted for upstream configuration in figure 4.3a, and downstream configuration in figure 4.3b.



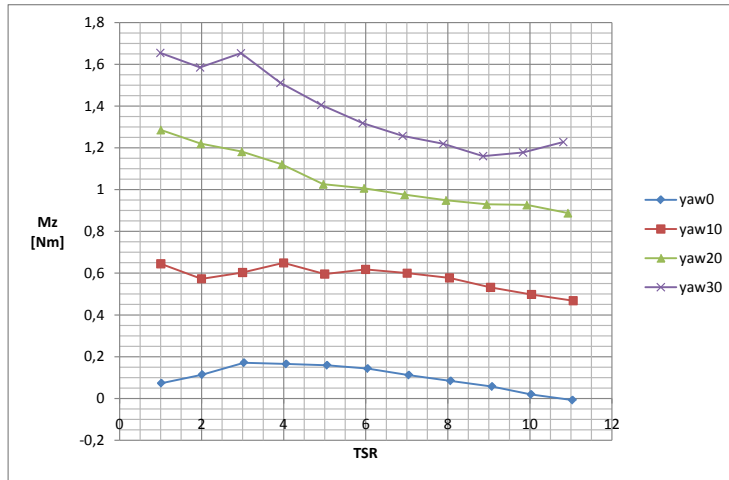
(a)  $C_T$  for upstream configuration



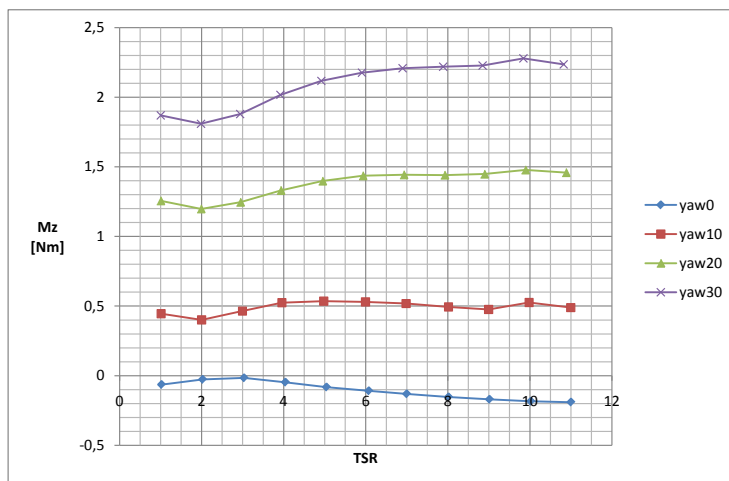
(b)  $C_T$  for downstream configuration

Figure 4.3: Thrust coefficients without contribution from tower and nacelle

The yaw moment,  $M_Z$  is also influenced by the tower and nacelle. Therefore this parameter is also plotted twice. The yaw moment for upstream configuration including the effect of the tower and nacelle is shown in figure 4.4a, and for the entire construction with downstream configuration in figure 4.4b. For the upstream and downstream configuration without the contribution to the yaw moment from the tower and nacelle see figures 4.5a and 4.5b respectively.

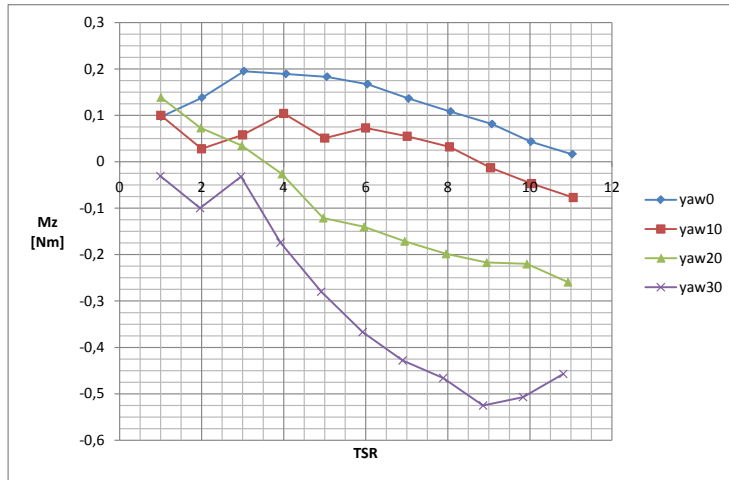


(a)  $M_Z$  for upstream configuration

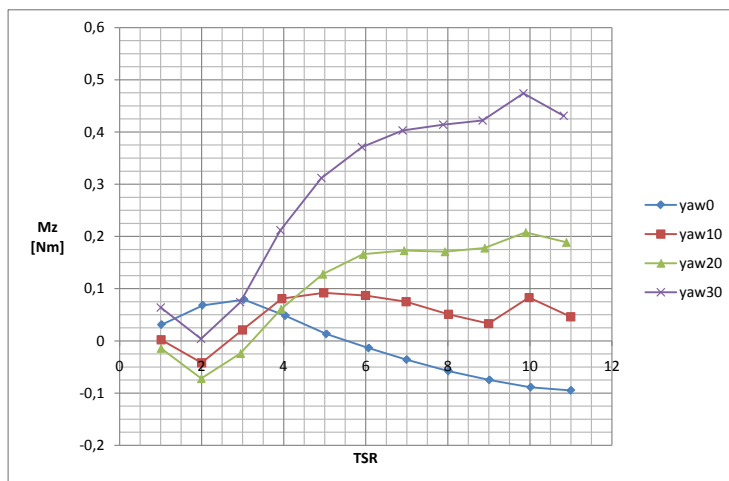


(b)  $M_Z$  for downstream configuration

Figure 4.4: Yaw moment including contribution from tower and nacelle



(a)  $M_Z$  for upstream configuration



(b)  $M_Z$  for downstream configuration

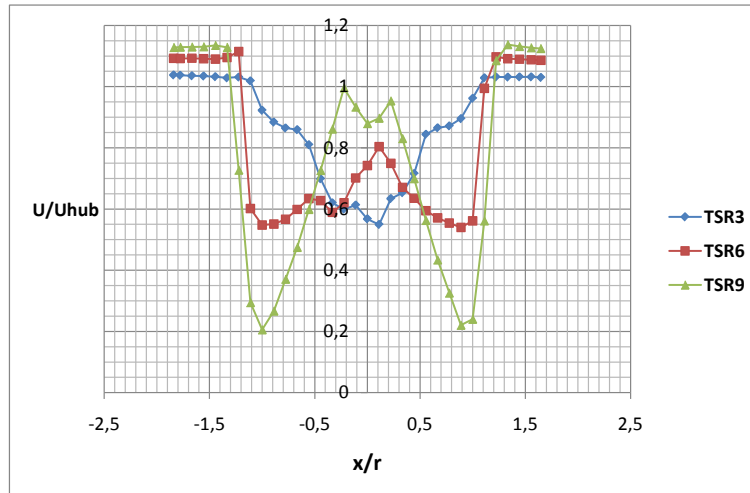
Figure 4.5: Yaw moment without contribution from tower and nacelle

## 4.2 Horizontal profiles

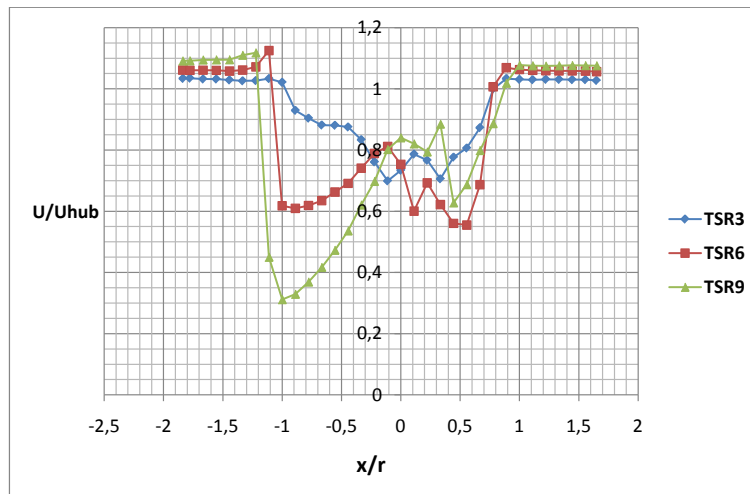
For each of the cases described in table 4.1 the horizontal profile has been measured. The velocity relative to the hub velocity for different distances in x direction are displayed in this section.

Figure 4.6 shows the clear difference between the various tip speed ratios that has been examined.

The horizontal velocity profiles for several distances behind the rotor plane for a



(a)  $\gamma = 0^\circ$

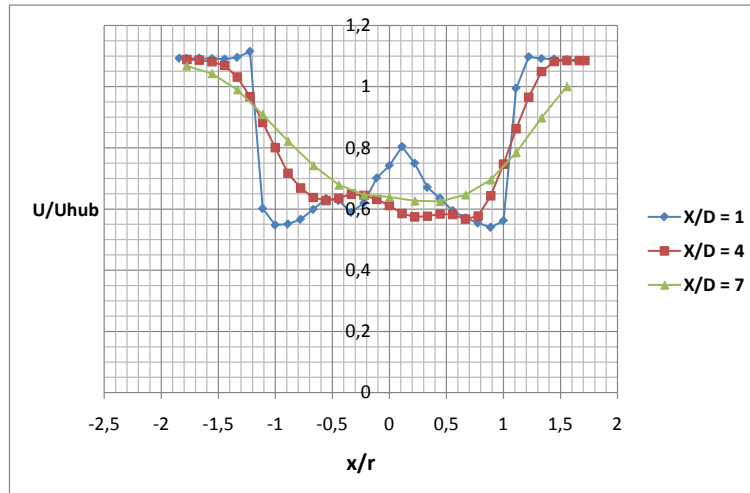


(b)  $\gamma = 30^\circ$

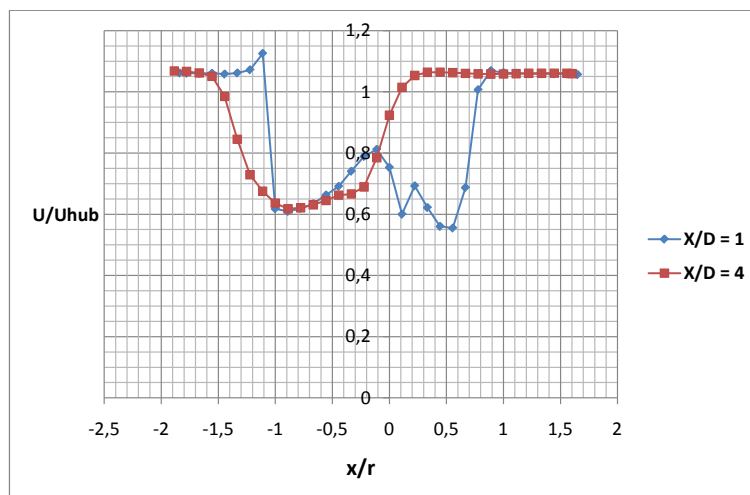
Figure 4.6: Horizontal velocity profile for  $X/D = 1$

wind turbine with constant operating condition  $\lambda = 6$  are displayed in figure 4.7. From this it is possible to see some of the wake development. In figure 4.7a the distance  $X/D = 7$  is also measured, but due to the limited amount of time in which these experiments were performed, this distance had to be neglected for the rest of the measurements.

Figures 4.8 and 4.9 shows the difference between  $\gamma = 0^\circ$  and  $\gamma = 30^\circ$  for different tip speed ratios and distances behind the rotor plane.

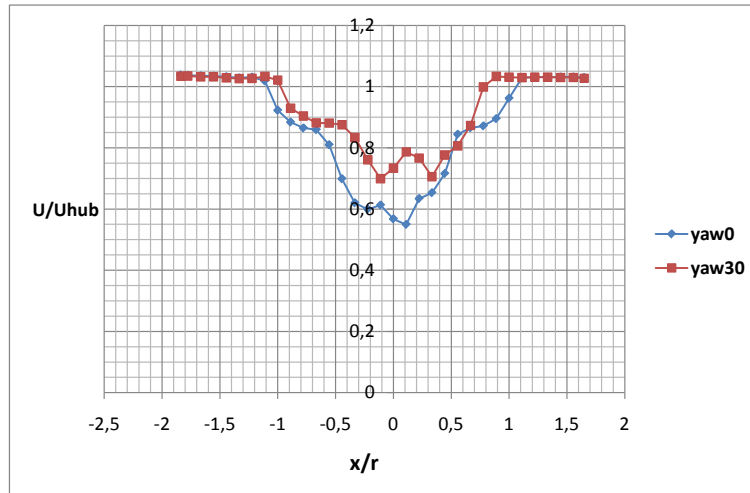


(a)  $\gamma = 0^\circ$

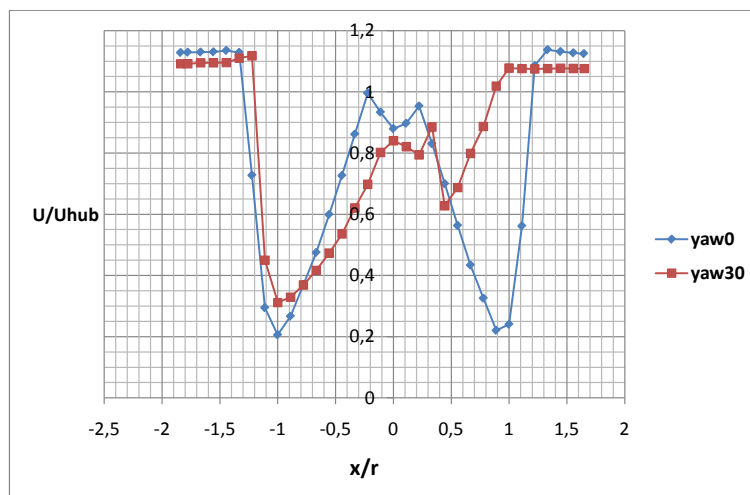


(b)  $\gamma = 30^\circ$

Figure 4.7: Horizontal profiles for different distances behind the rotor plane for  $\lambda = 6$



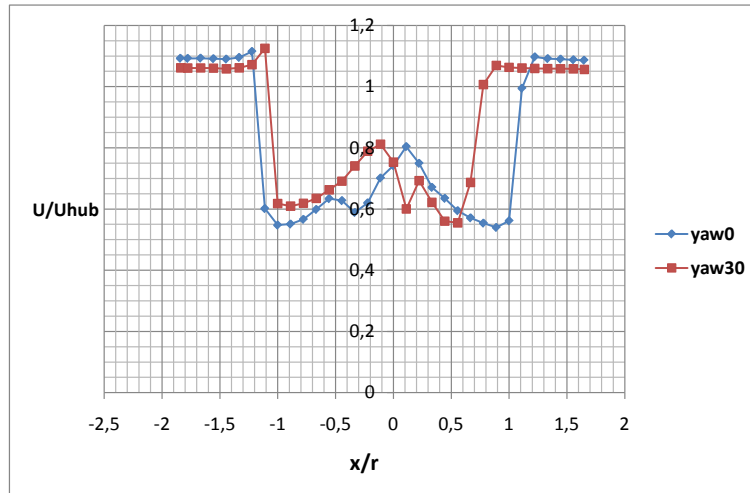
(a)  $\lambda = 3$



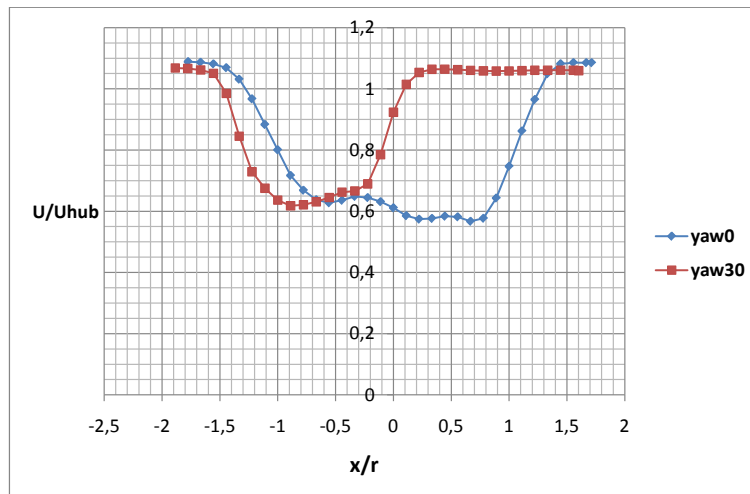
(b)  $\lambda = 9$

Figure 4.8: Horizontal profiles for different yaw angles at  $X/D = 1$





(a)  $\lambda = 6$  and  $X/D = 1$



(b)  $\lambda = 6$  and  $X/D = 4$

Figure 4.9: Horizontal profiles for different yaw angles

### 4.3 Velocity contours

For the cases described in table 4.1 the velocity field behind the wind turbine has been measured. These results follow in the contour plots in this section. All the contour plots are done with the same distance between each point measured. These distances, both in height ( $\Delta z$ ) and width ( $\Delta x$ ) are always  $10\text{cm}$  evenly distributed.

The tower for  $\gamma = 30^\circ$  is no longer at the vertical position  $x/r = 0$ . When rotating

the balance the tower position is changed and will be at  $x/r = 0.15$ .

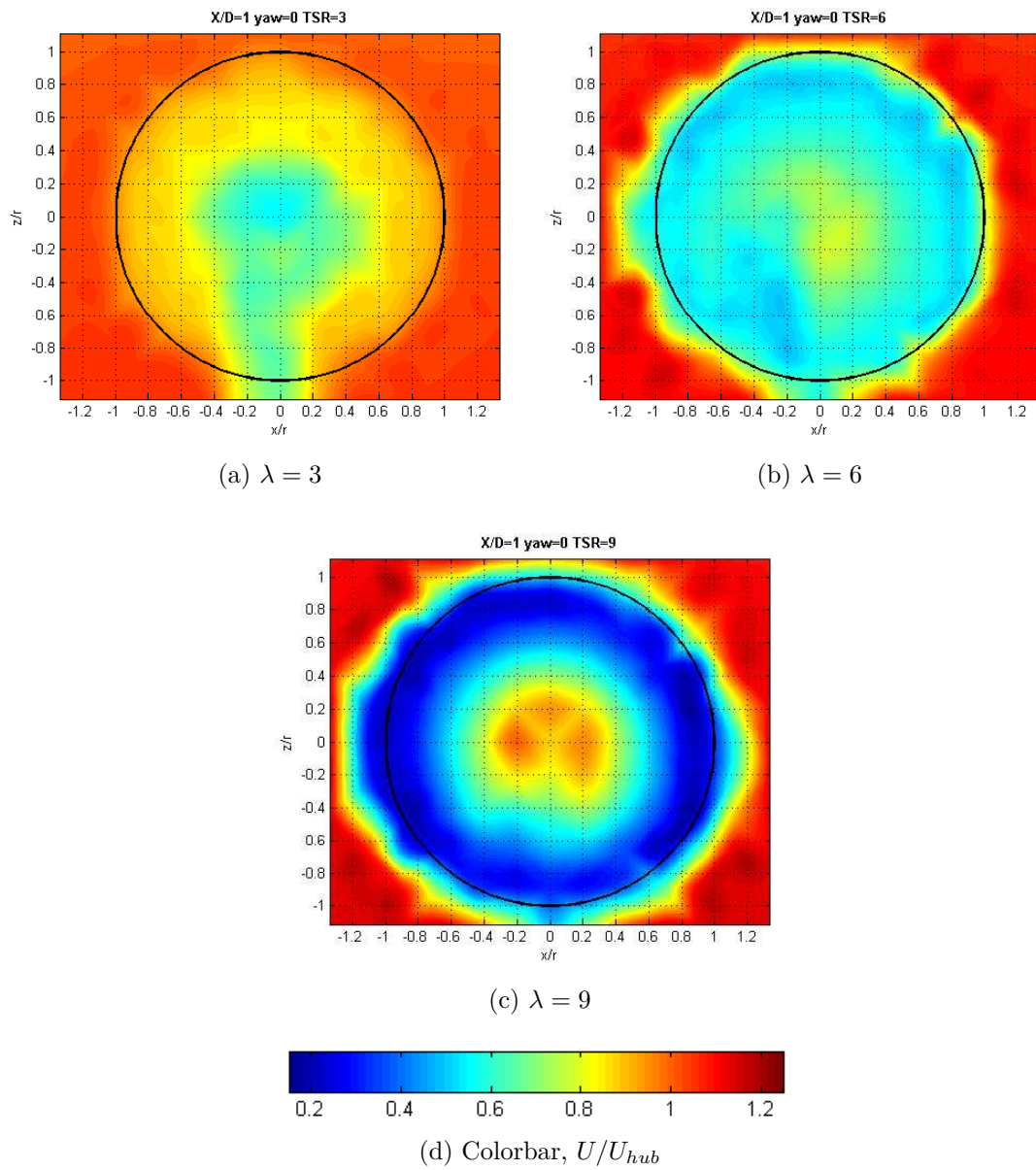


Figure 4.10: The velocity field at  $X/D = 1$  and  $\gamma = 0^0$

The velocity contours for  $X/D = 1$  and  $\gamma = 0^0$  are shown in figure 4.10. The size of the grid is the same for all three plots, and the colorbar displays the distribution of  $U/U_{hub}$ .

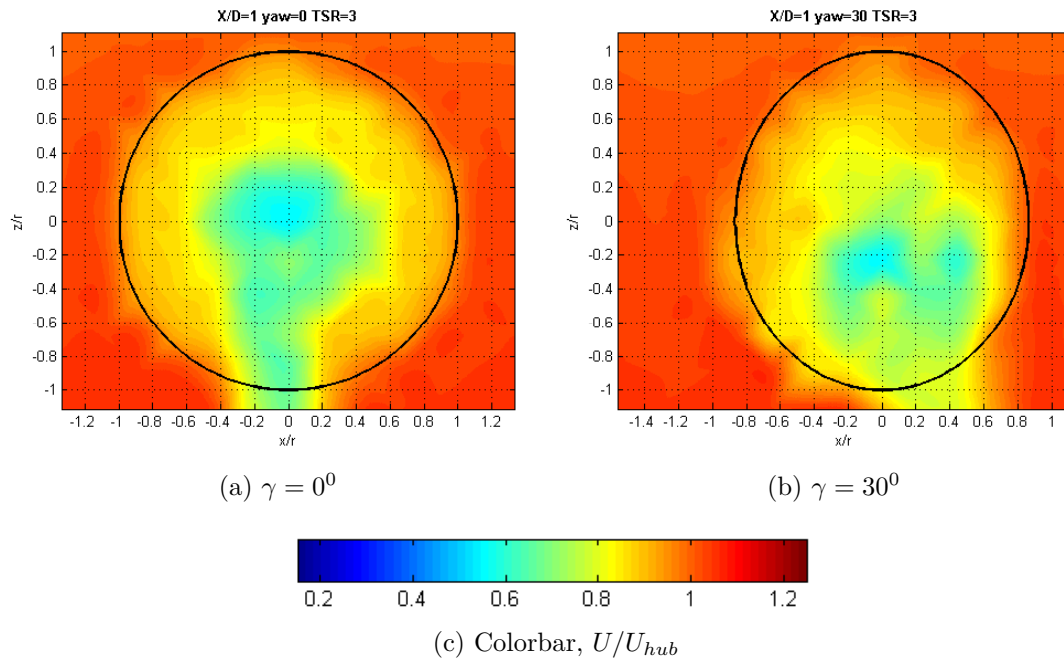


Figure 4.11: The velocity field for  $X/D = 1$  and  $\lambda = 3$

The difference between the velocity field for  $\gamma = 0^\circ$  and  $\gamma = 30^\circ$  with a tip speed ratio of 3 and one diameter behind the rotor plane can be seen in figure 4.11. The rotor plane is marked in the different plots, and for the cases where  $\gamma = 30^\circ$  the rotor plane will no longer be a circle. The rotor plane now has an elliptic form, since the grid measurements are done parallel to the rotor plane at  $\gamma = 0^\circ$ .

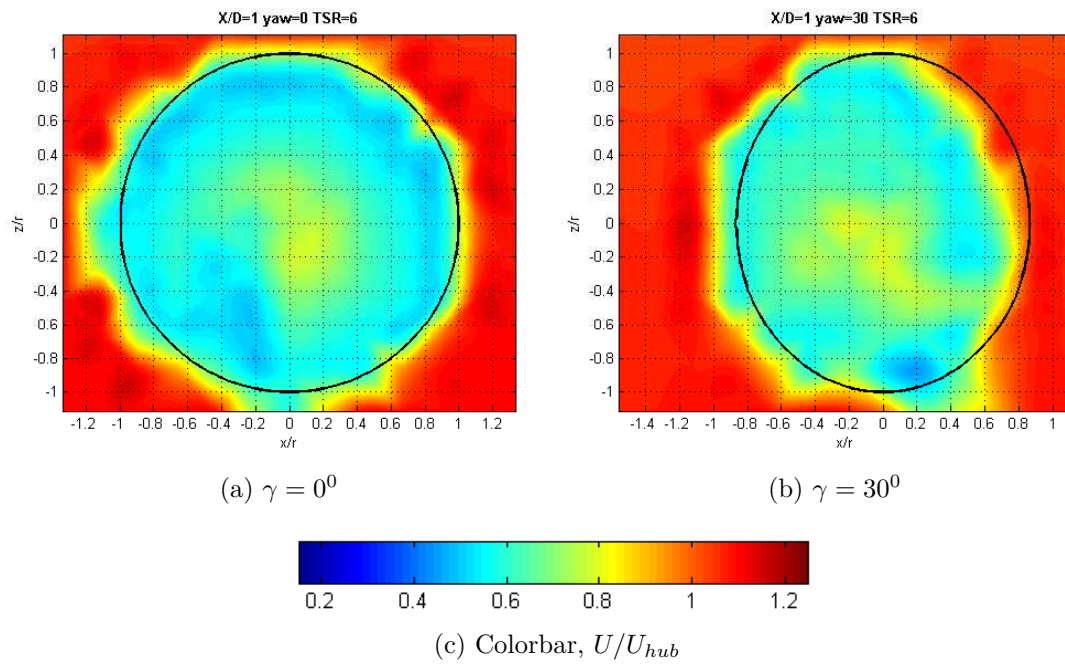


Figure 4.12: The velocity field for  $X/D = 1$  and  $\lambda = 6$

Figure 4.12 shows the velocity field for  $\lambda = 6$  and  $X/D = 1$  with two different yaw angles. Again the plot for  $\gamma = 30^\circ$  has a smaller rotor plane area than the one with  $\gamma = 0^\circ$ .

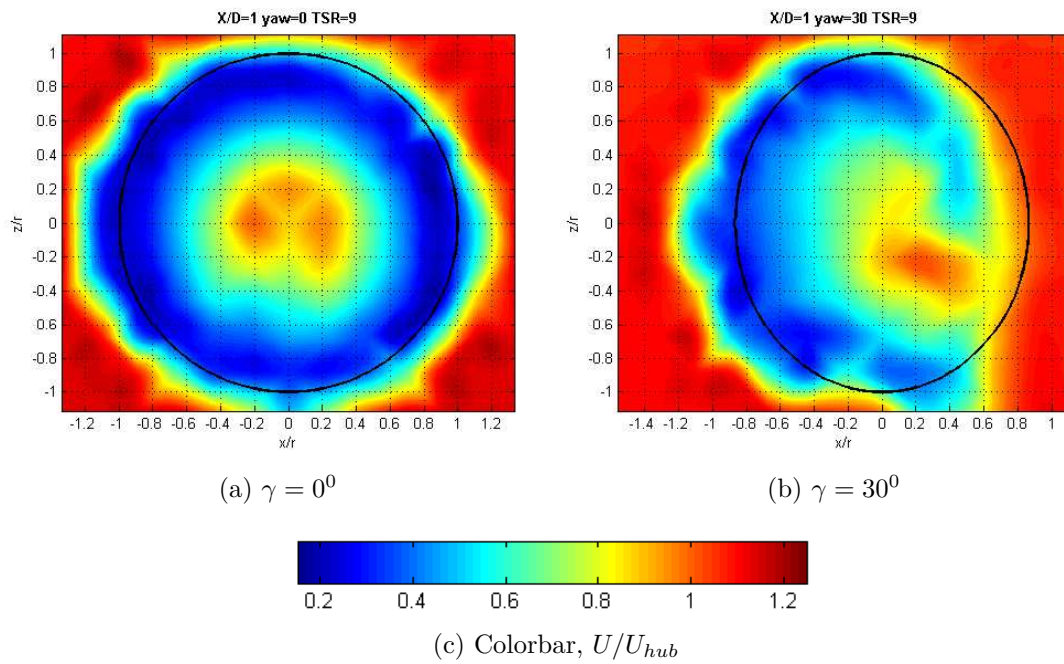


Figure 4.13: The velocity field for  $X/D = 1$  and  $\lambda = 9$

Also the velocity field for the two different yaw angles are found for  $\lambda = 9$  and  $X/D = 1$ . This is shown in figure 4.13.

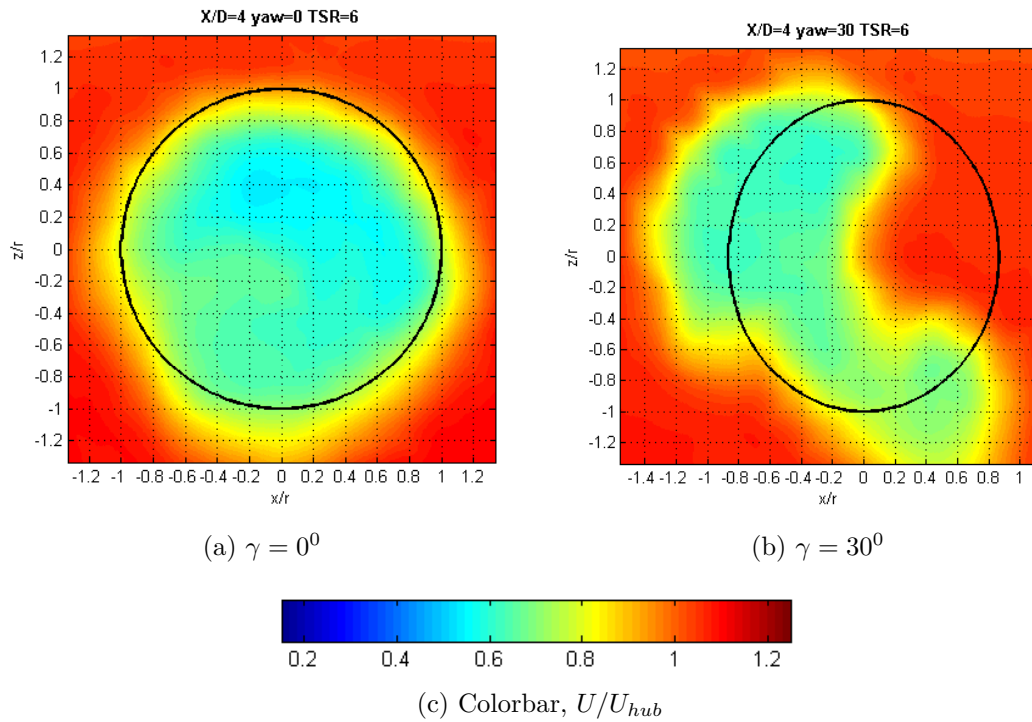


Figure 4.14: The velocity field for  $X/D = 4$  and  $\lambda = 6$

For  $X/D = 4$  the velocity field was determined for  $\lambda = 6$  and  $\gamma = 0^\circ$  and  $30^\circ$ . This is displayed in figure 4.14. The size of the field measured was larger in the  $z$  direction for this case. The reason for this was that the vertical velocity plots (see Appendix C) indicated that the wake had expanded so that the grid had to be increased in  $z$  direction to cover the entire wake.

For all the measurements with  $\gamma = 30^\circ$  the measured grid has been moved  $1 \cdot \Delta x$  to the left seen from an upstream position. This is due to the deflection of the wake found in the horizontal profiles from the previous section, 4.2.

## 5 Discussion

### 5.1 Performance characteristics and yaw moment

When changing the yaw angle of a wind turbine, the angle of attack will be affected. This results in the aerodynamic behavior of the blade being different, so that the performance characteristics will vary according to  $\gamma$ .

Previous measurements has been conducted of the yaw moment angular velocity by Nishizawa et al. [16] on a small horizontal axis wind turbine with tail fins and five bladed rotor.

#### 5.1.1 Power coefficient

The power coefficient measured for the different yaw angles coincide well with previous test performed by Karlsen [10] and Adaramola [2]. Also it is clear from the graphs that  $C_P$  decrease as the yaw angle increase. The area of the rotor plane that is perpendicular to the incoming wind is reduced, and therefore the wind turbine cannot utilize as much of the kinetic energy in the wind. When the yaw angle is  $\gamma = 30^\circ$  the area seen from an upstream position parallel to the wind direction is reduced with 13.4% compared to a yaw angle of zero degrees.

As can be seen from the power coefficient curves,  $C_P$  is approximately the same for upstream and downstream configuration. It was expected that the downstream wind turbine should have a lower efficiency than the upstream machine. The same blades are used for both configurations, so this can be one reason for this equality. A probable cause is that the tower and nacelle does not create wind shading at a larger extend for the downwind configuration compared to the upwind setup.

The power coefficient reaches maximum value at  $\lambda \approx 6$ . This was expected, since the design tip speed ratio is 6.

At low tip speed ratios the blades experience stall. Therefore the power coefficient is low at low  $\lambda$ . At high tip speed ratios above the design  $\lambda$ , the power coefficient decrease. This is due to the root of the blades experiencing negative angle of attack and providing power to the flow instead of subtracting it.

When the yaw angle is increased, the power coefficient decrease. This is due to the reduced projected rotor area as mentioned earlier, but also the reduced effective wind speed component that interacts with the rotor blades.

For low tip speed ratios the power coefficient is not very sensitive to the yaw angle, but as the  $TSR$  increase the dependency of  $C_P$  on  $\gamma$  increase. The power loss is also small for  $\gamma = 10^\circ$  but increase for  $\gamma = 20^\circ$  and  $30^\circ$ . This relation is not linear

as the growth in reduced  $C_P$  is larger between  $\gamma = 10^\circ$  and  $\gamma = 20^\circ$  than the difference between zero yaw and a yaw angle of  $10^\circ$ .

The run-away point where the wind turbine no longer extract energy from the wind for a yaw angle of  $0^\circ$  is at  $\lambda \approx 11.2$  for both upstream and downstream configuration, see figure 4.1. As the yaw angle increase, the run-away point appears at lower  $TSR$  and reduce the operating range of the turbine.

### 5.1.2 Thrust coefficient

The thrust coefficient reaches a value greater than 1 even after the tower and nacelle effects have been subtracted, see figure 4.3a and 4.3b. Previous studies performed by Karlsen [10] and Adaramola [2] have shown a similar development of  $C_T$ . For real life wind turbines, the thrust coefficient will be below one. For the test turbine in the wind tunnel the blockage ratio will have an effect on this coefficient. Therefore it is possible to get a thrust coefficient higher than 1 due to the local velocity increase at the rotor plane as a consequence of the turbine being in a closure.

The general pattern in the  $C_T$  curves for upstream and downstream wind turbine configuration shown in figure 4.3, is that for increasing yaw angle, the thrust coefficient decrease. The reason for this is the reduction of the effective freestream velocity, the rotor swept area and the deflection of the wake from the centerline. For low tip speed ratios, the yaw angle has small effects on the thrust. In figure 4.3 it can be seen that the reduction in thrust is very small for  $\gamma = 10^\circ$  but larger for  $\gamma = 20^\circ$  and  $30^\circ$ .

The thrust coefficient is very similar for the downstream and upstream configuration. As can be seen, when subtracting the tower and nacelle effects, this reduce the thrust coefficient with approximately 20% for  $\lambda = 3$  and 8% for  $\lambda = 9$  and  $\gamma = 0^\circ$  for upstream configuration.

### 5.1.3 Yaw moment

For a yaw angle of zero degrees, the yaw moment should in theory be zero. This is not the case for either upstream or downstream configuration as can be seen in figures 4.5a and 4.5b.

When the moment is located in an upstream position,  $M_Z$  has the same shape for  $\gamma = 0^\circ$  as for  $\gamma = 10^\circ, 20^\circ$  and  $30^\circ$ . This indicates that the turbine has been operating with a positive yaw angle that might be in the order of  $2^\circ$  to  $4^\circ$ .



For the downstream configuration the yaw moment has the opposite shape of  $M_Z$  for  $\gamma = 10^\circ, 20^\circ$  and  $30^\circ$ . Therefore it is reasonable to assume that the yaw angle initially had a negative value that must have been approximately  $-2^\circ$  to  $-4^\circ$ .

When the upstream measurements has been done, the yaw angle has then been of a larger magnitude than displayed in the figures 4.4a and 4.5a. For the downstream configuration it has been the other way around, so that the yaw angles specified in the plots 4.4b and 4.5b are in reality lower.

For upstream configuration the yaw moment is unstable for  $\gamma = 10^\circ$  up to approximately  $\lambda = 9$ . When the yaw angle increase, the tip speed ratio where there is a shift from unstable to stable yaw moment decrease. At a yaw angle of  $20^\circ$  the yaw moment is only unstable up to a  $TSR$  of approximately 3.5. For the maximum yaw angle explored in these measurement,  $\gamma = 30^\circ$ , the yaw moment is unconditionally stable. This can all be seen in figure 4.5a. As mentioned, for a yaw angle of zero degrees  $M_Z$  should in theory be zero. For the upstream setup, the yaw moment at  $\gamma = 0$  is unconditionally unstable. This coincide well with the assumption of that the real  $\gamma$  is approximately  $2^\circ - 4^\circ$ . This means that for small yaw angles the upstream wind turbine will have a yaw moment that tends to rotate the rotor plane out of the wind. As the yaw angle increase, the point where  $M_Z$  becomes stabilizing for the system appears at decreasing values for the tip speed ratio.

For the downstream wind turbine configuration it can be seen from the figures 4.5a and 4.5b that the yaw moment is on a general basis, more stable than for the upstream setup. For a yaw angle of  $10^\circ$  the yaw moment is unstable from  $\lambda = 0$  to  $\lambda = 2.6$ . When the yaw angle is increased to  $20^\circ$ , the system is unstable up to a tip speed ratio of 3.2. Between  $\gamma = 10^\circ$  and  $\gamma = 20^\circ$  the tip speed ratio where the yaw moment is stable increase. This is opposite of what was found for the upstream configuration. Still, for  $\gamma = 30^\circ$  the yaw moment is unconditionally stable. As mentioned previously, the yaw moment should be zero for a yaw angle of zero degrees. Since this is not the case, it has been assumed that the yaw angle for downstream configuration is negative in the area  $-2^\circ$  to  $-4^\circ$ . This agrees with the result shown in figure 4.5b.  $M_Z$  is unstable from  $\lambda = 0$  to  $\lambda = 5.5$  for what should be  $\gamma = 0$ , and at higher tip speed ratios it tends to turn the rotor plane in to the wind.

The tower and nacelle are massive, and therefore they have a large effect on the yaw moment. As can be seen in figure 4.4a the contribution from the tower and nacelle have an unstabilizing effect on  $M_Z$  for the upstream configuration, and cause the yaw moment to be unconditionally unstable for all yaw angles measured. For the downstream setup these effect has the opposite result, it contributes to the yaw moment being stable for all yaw angles and tip speed ratios. From this it is possible to conclude that the tower and nacelle has a positive effect on the yaw moment for the downstream wind turbine system.

### 5.1.4 Comparison with calculations using the blade element momentum method

A previous study of the yaw moment on a wind turbine has been performed using the blade element momentum method for oblique inflow [13]. The machine considered here was a downstream horizontal axis wind turbine with the same dimensions and blades as the one used for the experiments in the wind tunnel in this thesis. From the previous study, the yaw angle was defined in the opposite direction than what has been done here. Therefore, when comparing results, the blade element momentum method calculations will have a negative yaw angle.

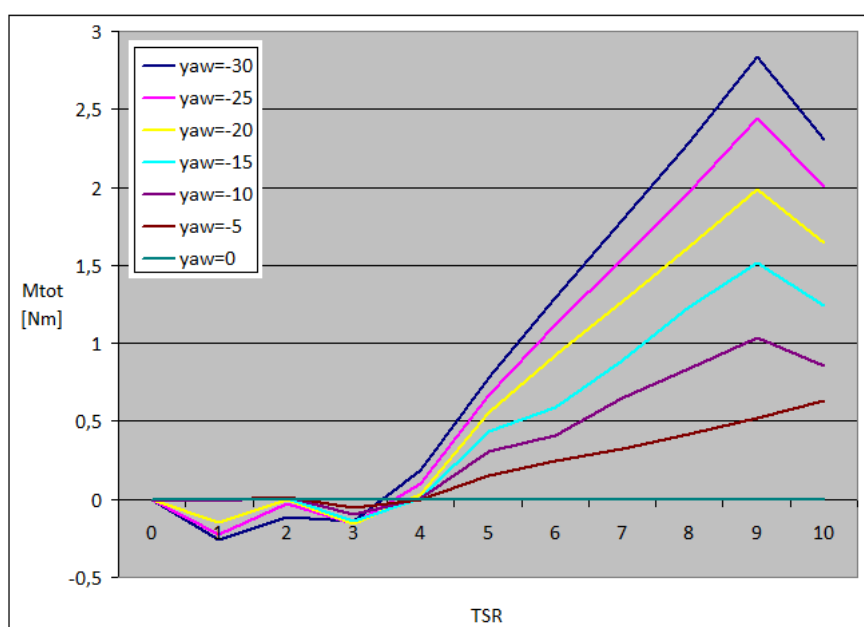


Figure 5.1: Total yaw moment calculated using BEM for oblique inflow and  $l = 15\%$  of tower height

When comparing figure 5.1 and 4.5b it is clear that the shape of the graphs are similar. The magnitude of the yaw moment on the other hand, is different with a factor of approximately 5.8. A possible reason for this deviation between measured and calculated results has been searched for with no luck. The calibration of the balance was checked by applying known weights and manually calculating the expected results from ForceLog. Measurements and calculations coincided well, but not all of the cells were tested. An inaccuracy in one of the cells responsible for measuring the yaw moment, or in the equipment used for the measurement for one of these cells is a possible explanation. If not, a deviation can have occurred when using the source code for the blade element momentum method with oblique inflow in matlab to calculate  $M_Z$ . Inaccuracies and simplifications made using the

blade element momentum method for oblique inflow are mentioned below. These limitations will cause a deviation between measurements in the wind tunnel and calculated results in matlab. However, they will not be of the magnitude that can explain the factor 5.8 difference in the yaw moment.

### **Inaccuracies in the blade element momentum method**

When using the blade element momentum method there are several factors that may cause inaccuracies in the calculations. It is assumed that the wind is stationary and uniform, and the lift and drag coefficients are calculated for a blade that is not rotating. There is a pressure drop across the wind turbine rotor for real turbines, but this is considered to be very small and is therefore not expected to have a large influence on the errors. It is also assumed that the pressure drop over the rotor plane is small for a wind turbine operating under yawed conditions. An approximation to the flow expansion function is used, and also the calculation of the skew angle,  $\chi$ , is simplified. During the iteration process it might occur a divergence of the values for the elements close to the hub. If this is the case the contribution from these elements are disregarded. For large thrust coefficients, Glauerts correction is applied to the calculations. This correction is valid for incoming wind perpendicular to the rotor plane, but is here used for turbines operating with yaw angle. The calculations are done assuming the Reynolds number is  $10^5$ . For the experiments performed in the wind tunnel the Reynolds number will be approximately  $Re = \frac{UD}{1.5 \cdot 10^{-5}} = 3 \cdot 10^5$ .

These simplifications and corrections will all part in the solution being less accurate.

## **5.2 Wake measurements**

The three different tip speed ratios that are explored in these measurements has been chosen because they describe different performance characteristics of the turbine. The low  $\lambda$  that has a value of approximately 3 describe stalled operation.  $\lambda \approx 6$  is for the optimum operation and  $\lambda \approx 9$  shows the flow when the model turbine act as a propeller.

Vertical profiles has also been measured for the different cases. This has been done for comparison with the velocity field measurement, and they are displayed in Appendix C.

### 5.2.1 The effect of tip speed ratio

For low tip speed ratio,  $\lambda \approx 3$ , the velocity deficit is highest near the hub. This can be seen in figures 4.6, 4.10a and 4.11. It can also be seen from these figures that the axial velocity at the outer part of the rotor plane is approximately 80% of the freestream velocity. This indicates that there is little interaction between the airflow and rotor, and most of the air passes through without being disturbed by the wind turbine blades. Since large parts of the air flows past the turbine without being affected by the rotor, less energy is extracted from the flow and the regime is characterized by low  $C_P$  and  $C_T$  as can be seen in figures 4.1a and 4.3a.

When  $\lambda \approx 6$ , the optimum  $TSR$ , the velocity deficit is more evenly distributed and stronger than for the low  $TSR$ . This can be seen in figure 4.10b. This shows that the rotor operates efficiently, and the energy is extracted uniformly from the flow.

For the high tip speed ratio,  $\lambda \approx 9$ , the radial variations in the velocity deficit are strong compared to the cases with lower  $TSR$ . This can be seen from the horizontal velocity profiles in figure 4.6. The outer part of the blade operate at low angles of attack, and is therefore not very efficient. The inner parts of the velocity field close to the hub, act as a propeller. This causes the rotor to add energy to the flow instead of subtracting it, and can be seen as a very small velocity deficit in the central part of the wake, see figure 4.10c. Even though the center and outer parts of the wake does not operate efficiently, the middle parts successfully exploit the energy in the wind to some extent. The thrust coefficient is high for this tip speed ratio, and it can be seen from figure 4.6 that the wake at  $X/D = 1$  has expanded more in this case than for those with a lower  $TSR$ .

As the tip speed ratio increase, the velocity gradients become stronger, and so does the turbulence levels.

### 5.2.2 Velocity field development

From figure 4.7a it can be seen that the wake width increase with streamwise distance from the rotor plane. As the wake width increase downstream, the velocity deficit decrease.

When the turbine is operating at optimum tip speed ratio, there is a sudden drop in velocity deficit near the tip of the blades, see figures 4.7a and 4.10b. Following this fall further downstream, it is seen to even out quickly. This is due to the entrainment from the freestream flow due to the tip vortices. There are strong mechanisms acting to make the velocity deficit even out as the wake develops

downstream, this can again be seen in figure 4.7a but also when comparing figures 4.12a and 4.14a that displays the velocity field.

Figure 4.14b clearly shows the rotation of the wake as it has moved  $4D$  downstream from the rotor plane.

### 5.2.3 Yaw angle effect

From figures 4.6b, 4.8 and 4.9 it can be seen that the model wind turbine deflects the wake towards the yawed direction. Comparing the velocity field for a yaw angle of  $0^0$  with  $\gamma = 30^0$  in figures 4.11 to 4.13 it can be concluded that the wake becomes asymmetrical. It can be seen from the same figures that there is a distinct reduction in wake width as well. This is due to the reduction in the rotor swept area as mentioned earlier.

For large yaw angles, the entrainment of momentum from the freestream to the wake is increased and the wake recovers faster. Therefore the expansion of the wake will be smaller for turbines operating in yawed inflow. See figures 4.7b and 4.14 where the expansion of the wake at  $X/D = 4$  for two different yaw angles is displayed.

The velocity field where  $\lambda \approx 9$  still has a part working as a propeller. This is no longer the center of the wake because of the asymmetry, and can be seen in figure 4.13b.

Figures 4.11 to 4.13 clearly shows a systematic asymmetric wake development and reduction of wake width when the wind turbine in oblique inflow. The deflection of the wake can be seen to increase with increasing  $\lambda$ . When the yaw angle is  $0^0$  the wake is symmetric about the vertical centerline of the rotor plane.

When the tip speed ratio is small,  $\lambda \approx 3$ , the velocity distribution is close to uniform for a yaw angle of  $0^0$ . When  $\gamma$  is changed to  $30^0$  the velocity field is still fairly uniform. This can be seen in figure 4.11. The main effect of the reduced power production in this case, will therefore be the reduced rotor plane area that is perpendicular to the incoming flow.

### 5.2.4 Comparison with other results

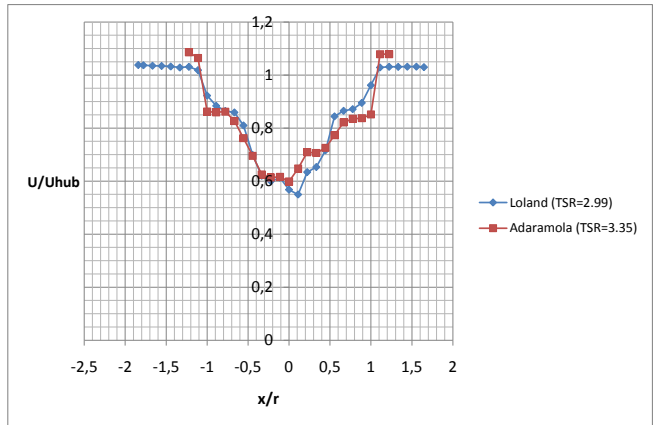
Measurements on the same test turbine used in this thesis are done earlier by Adaramola [2]. The results from the horizontal profiles obtained previously are compared to those found in this thesis.

In figure 5.2 that the measurements coincide well, and the small variations can be caused by the difference in tip speed ratio. The graphs are a bit deflected in

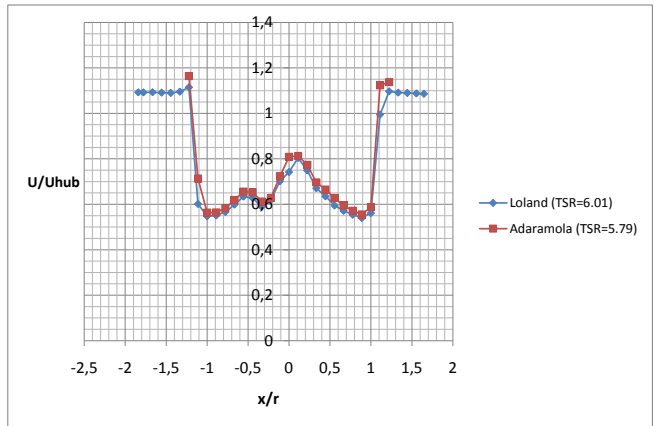
relation to each other. The reason for this can be that the yaw angle is not exactly zero, as mentioned previously.

The difference in yaw angle for the measurement comparison is clear in figure 5.3, where the graphs again have the same form, but are clearly shifted in relation to each other. The difference in magnitude of the normalized velocity can again be explained by different tip speed ratios.

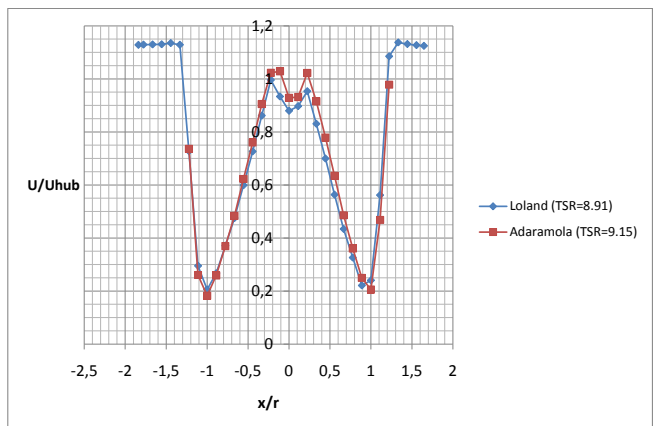
For a distance behind the rotor plane of  $X/D = 4$  and  $\gamma = 0^\circ$  a comparison of the horizontal velocity profiles can be seen in figure 5.4. The small deflection in the normalized velocity component can again be explained by different tip speed ratios. The shape of the graphs is very similar, and there does not seem to be any large difference in the yaw angle that is supposed to be zero in both cases.



(a)  $\lambda \approx 3$

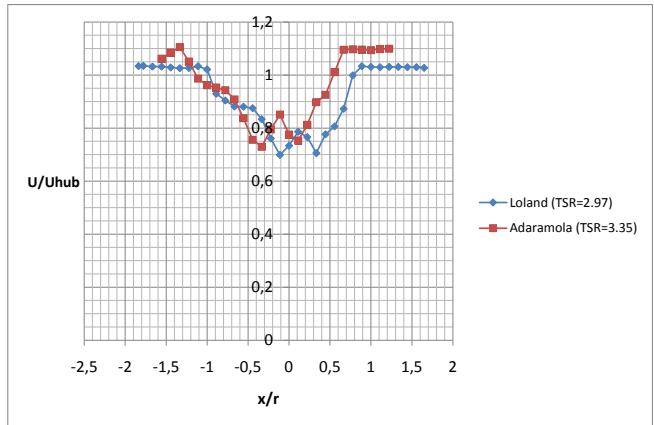


(b)  $\lambda \approx 6$

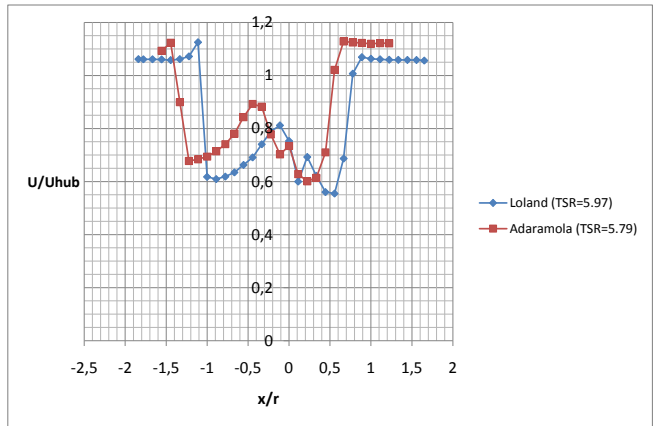


(c)  $\lambda \approx 9$

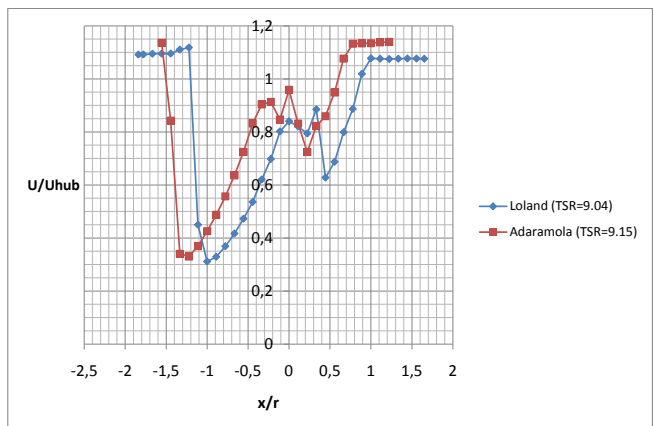
Figure 5.2: Comparison of data for  $X/D = 1, \gamma = 0^0$



(a)  $\lambda \approx 3$



(b)  $\lambda \approx 6$



(c)  $\lambda \approx 9$

Figure 5.3: Comparison of data for  $X/D = 1, \gamma = 30^0$



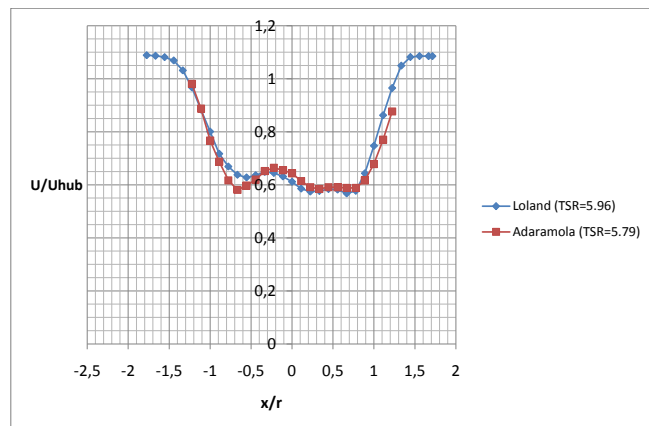


Figure 5.4: Comparison of data for  $X/D = 4, \gamma = 0^0$  and  $\lambda = 6$

## 6 Conclusion

For increasing yaw angle, both power production of the wind turbine and thrust force is severely decreased which can have a serious effect on offshore floating constructions. The yawing mechanism here will be more complex than for onshore turbines, and the units may operate in yawed conditions for long periods during production.

For yawed operation, the wake is deflected towards the yawed direction. This is not dependent on the tip speed ratio. A deflection of the wake can be beneficial for turbines further downstream, since the wake will not influence the flowfield this turbine sees to a great extent. Also, the wake will be narrower for a wind turbine operating with oblique inflow, compared to operation with  $\gamma = 0^\circ$ .

Three different regimes have been explored. The low tip speed ratio area where the blades are partly stalled, optimum  $TSR$  where the turbine is operating under design conditions and the high tip speed ratio regime.

The near wake area behind the wind turbine is strongly dependent of the tip speed ratio and yaw angle. For the partly stalled regime, the thrust and power coefficients are low. This results in the velocity defect being small. At the outer parts of the rotor plane, the normalized velocity is close to 1. This implies that little energy is extracted from the flow, and the air mostly passes the wind turbine blades undisturbed.

When the tip speed ratio is close to 6, which is the optimum  $\lambda$  for the test turbine, the power coefficient is high and the thrust coefficient is modest. Over the rotor plane, the velocity deficit is uniformly distributed, which means that most parts of the blades efficiently extract power from the incoming flow. For zero yaw and  $\gamma = 30^\circ$  four rotor diameters downstream from the rotor plane, it is found that the wake has expanded due to the high energy extraction from the wind. The velocity deficit has also become more uniform.

For the high tip speed ratio regime, where  $\lambda \approx 9$ , the thrust coefficient is high compared to the lower tip speed ratios. The power coefficient is low, so the wind turbine does not efficiently draw power from the wind. In the rotor area near the hub the magnitude of the velocity field is similar to the freestream velocity. This is because the inner parts of the blades experience a negative angle of attack, and are therefore adding energy to the flow instead of subtracting it.

The power and thrust coefficient is similar for upstream and downstream configuration. One reason for this similarity can be that the same turbine and turbine blades were used in both cases. The yaw moment is also in the same magnitude for the two different setups. Still, the yaw moment is generally more stable for the downstream configuration than for the upstream alternative.

The effect of the tower and nacelle on the yaw moment was seen to be large since the construction is massive. These worked to increase the stability of the downstream wind turbine, but made the upstream turbine yaw moment unconditionally unstable.

For upstream configuration there seems to be a relation between the increase in yaw angle and the decrease in necessary tip speed ratio to get a stable system. This was not the case for the downstream setup, but for this setup the yaw angle and tip speed ratio could generally be lower and still cause a stabilizing moment compared to the upstream configuration. Both cases had an unconditionally stable yaw moment for a yaw angle of  $30^{\circ}$  and partially unstable system for yaw angles lower than this. The downstream wind turbine configuration has a generally more stable free yaw moment than an upstream configuration.

## 7 Further work

The physics in the wind turbine wake is not yet fully understood. More measurements should be carried out, and at several distances behind the rotor plane. In this thesis it was mainly  $X/D = 1$  that was explored, but cases up to  $X/D = 7$  or 10 should be carried out and analyzed. Both with and without yaw angle on the wind turbine.

Only one yaw angle in addition to zero yaw was used in the velocity field measurements. More yaw angles should be explored for different operating conditions. If this is carried out, it will be easier to plan a wind park where some turbines operate in yawed condition, to increase power production from downstream units and maximize the power output from the park.

Generally there are few experiments performed on downwind turbines. If these are to be a real alternative for offshore floating wind energy, this must be explored further. The power and thrust curves, as well as yaw moment should definitely be experimented on for several yaw angles and various tip speed ratios. Ideally these experiments would be performed on a downwind construction, not an upwind turbine rotated  $180^\circ$  as has been done in this case. Then it could be possible to get an impression of how the downwind wind turbine should be constructed to optimize production and minimize fatigue and downtime.

## References

- [1] Krogstad P.-Å. Adaramola, M.S. Experimental investigation of wake effects on wind turbine performance. *Renewable Energy*, 36(8):2078–2086, 2011. cited By (since 1996) 0.
- [2] Krogstad P.-Å. Adaramola, M.S. Performance and near wake measurements of a model horizontal axis wind turbine. under Review, 2011.
- [3] J.F. Ainslie. Calculating the flowfield in the wake of wind turbines. *Journal of Wind Engineering and Industrial Aerodynamics*, 27(1-3):213 – 224, 1988.
- [4] Tony Burton, David Sharpe, Nick Jenkins, and Ervin Bossanyi. *Wind Energy - Handbook*. John Wiley & Sons Ltd, 2001.
- [5] Leonardo Chamorro and Fernando Porté-Agel. A wind-tunnel investigation of wind-turbine wakes: Boundary-layer turbulence effects. *Boundary-Layer Meteorology*, 132:129–149, 2009. 10.1007/s10546-009-9380-8.
- [6] Bak C. Fuglsang, P. Development of the risø wind turbine airfoils. *Wind Energy*, 7(2):145–162, 2004. cited By (since 1996) 16.
- [7] Per Åge Krogstad. Private communication, 2011.
- [8] Martin O. L. Hansen. *Aerodynamics of wind turbines*. Earthscan, second edition, 2008.
- [9] Erich Hau. *Wind Turbines - Fundamentals, Technologies, Application, Economics*. Springer-Verlag Berlin Heidelberg, second edition, 2006.
- [10] J.A. Karlsen. Performance calculations for a model turbine. Master’s thesis, Norwegian university of science and technology, 2009.
- [11] Jon Amund Karlsen. Performance calculations for a model turbine. Master’s thesis, Norwegian University of Science and Technology, 2009.
- [12] P.-Å Krogstad and J.A. Karlsen. An experimental and numerical study of the performance of a model turbine. under Review, 2011.
- [13] Kari Medby Loland. Vindturbin med nedstrøms rotor. Prosjektoppgave NTNU, 2011.
- [14] Takao Maeda, Yasunari Kamada, Jun Suzuki, and Hideyasu Fujioka. Rotor blade sectional performance under yawed inflow conditions. *Journal of Solar Energy Engineering*, 130(3):031018, 2008.
- [15] J. F. Manwell, J. G. McGowan, and A. L. Rogers. *Wind Energy Explained - Theory, Design and Application*. John Wiley & Sons Ltd, 2003.

- [16] Tokuyama H.b Nakajo Y.a Ushiyama I.c Nishizawa, Y.a. Yaw behavior of horizontal-axis small wind turbines in an urban area. *Wind Engineering*, 33(1):19–30, 2009. cited By (since 1996) 0.
- [17] D.R.S. Verelst and T.J. Larsen. Yaw stability of a free-yawing 3-bladed downwind wind turbine. Wind Energy Research. <http://windenergyresearch.org/?p=398>, 2010.
- [18] S. Yoshida. Performance of downwind turbines in complex terrains. *Wind Engineering*, 30(6):487–502, 2006. cited By (since 1996) 5.

# A Learning by doing; small wind tunnel measurements

To learn the experimental techniques and the use of a wind tunnel, introductory measurements were done in a small open jet wind tunnel at the Department of Energy and Process engineering at The Norwegian University of Science and Technology. The fan can provide air velocities of up to  $30m/s$  within the test section. The length of the tunnel is  $1m$  and the width and height are both  $0.45m$ .

The equipment that is to be used:

- Manometer
- Amplifier
- Pressure transducer
- Software LabView, GenLog
- Pitot tube

## A.1 Atmospheric pressure

First the atmospheric pressure has to be calculated. This is done by the use of a mercury column where the height of mercury is found in  $mm$ . Then the formula (A.1) is used to calculate the pressure at the particular day.

$$P_{atm} = \rho_{mercury}gh_{mercury} \quad (A.1)$$

The atmospheric pressure is used to calculate the air density for the measurements.

## A.2 Manometer

It is important to remember that the manometer should be in level before adjusting the methylated spirit column to zero.

The height of the methylated spirit column in the manometer can be measured at different slope relations. To find out which slope that should be used, one has to assume the maximum velocity that would be obtained within the test section.

When a maximum velocity is assumed, the dynamic pressure can be calculated from:

$$P_{dyn} = \frac{1}{2}\rho_{air}U_{\infty}^2 \quad (\text{A.2})$$

and the column height of the methylated spirit can be found by:

$$\begin{aligned} P_{dyn} &= \rho_{MethylatedSpirit}gh_{MethylatedSpirit} \\ \Rightarrow h_{MethylatedSpirit} &= \frac{P_{dyn}}{\rho_{MethylatedSpirit}g} \end{aligned} \quad (\text{A.3})$$

In these experiments  $U_{max}$  is assumed to be  $20m/s$ . This gives  $h_{MethylatedSpirits} = 30,3mm$  and the slope used is  $1 : 5$ .

A long circular cylinder was placed horizontal in the wind tunnel. The measurements were performed at a distance of  $35cm$  behind the center of the cylinder. The height from the floor of the test section to the center of the cylinder, with a diameter of  $D_{cyl} = 5cm$ , was measured to be  $227mm$ . The height displayed in the vertical velocity plots in the figures A.2, A.4 and A.5 is related to the pitot tube. When the height is zero, the pitot tube is at the lowest point possible with the instrument used, and this is  $80mm$  above the floor of the test section. This implies that in the velocity plots the cylinder centre is at  $227mm - 80mm = 147mm$  above the floor of the test section.

The measurements were conducted during two days. The aim was to understand and be able to use the equipment that is necessary to do experiments in a wind tunnel.

### A.3 Day 1, 3/2 - 2011

Atmospheric pressure:

- $h_{mercury} = 748,7mm$
- $P_{atm} = 99491,94Pa$

The calibration on the first day were conducted twice to better understand the process and see if there is a significant difference between the two calibration constants obtained.

The first and second calibration curves can be seen in figure A.1a and A.1b respectively. The data for the first calibration can be found in table A.1 and the second in table A.2.

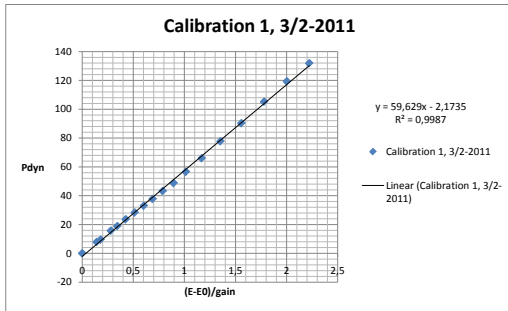


Table A.1: Calibration 1, day 1

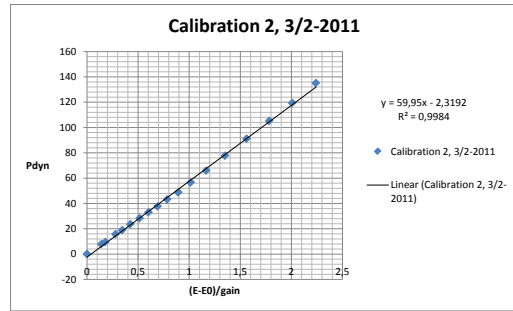
Nr	T [0C]	rho_air	E [V]	(E-E0)/gain	h_MetSp	Pdyn
1	19,1	1,1865959	-9,268	0	0	0
2	20	1,1829529	-8,131	0,142125	5	7,848
3	21	1,1789313	-7,826	0,18025	6	9,4176
4	20,7	1,1801349	-7,021	0,280875	10	15,696
5	20,8	1,1797335	-6,515	0,344125	12	18,8352
6	21	1,1789313	-5,86	0,426	15	23,544
7	20,9	1,1793323	-5,154	0,51425	18	28,2528
8	21	1,1789313	-4,446	0,60275	21	32,9616
9	21	1,1789313	-3,753	0,689375	24	37,6704
10	21,3	1,1777302	-2,961	0,788375	27,5	43,164
11	21	1,1789313	-2,106	0,89525	31	48,6576
12	21,1	1,1785307	-1,146	1,01525	36	56,5056
13	20,9	1,1793323	0,089	1,169625	42	65,9232
14	21,1	1,1785307	1,556	1,353	49,5	77,6952
15	21	1,1789313	3,192	1,5575	57,5	90,252
16	21	1,1789313	4,973	1,780125	67	105,1632
17	20,9	1,1793323	6,75	2,00225	76	119,2896
18	20,9	1,1793323	8,505	2,221625	84	131,8464

Table A.2: Calibration 2, day 1

Nr	T [0C]	rho_air	E [V]	(E-E0)/gain	h_MetSp	Pdyn
1	19	1,1870021	-9,266	0	0	0
2	21	1,1789313	-8,137	0,141125	5	7,848
3	21,2	1,1781303	-7,834	0,179	6	9,4176
4	21,2	1,1781303	-7,029	0,279625	10	15,696
5	21	1,1789313	-6,506	0,345	12	18,8352
6	21,2	1,1781303	-5,876	0,42375	15	23,544
7	21,2	1,1781303	-5,144	0,51525	18	28,2528
8	21,3	1,1777302	-4,447	0,602375	21	32,9616
9	21,3	1,1777302	-3,731	0,691875	24	37,6704
10	21,3	1,1777302	-2,983	0,785375	27,5	43,164
11	21	1,1789313	-2,113	0,894125	31	48,6576
12	21,2	1,1781303	-1,142	1,0155	36	56,5056
13	21,2	1,1781303	0,075	1,167625	42	65,9232
14	21,2	1,1781303	1,546	1,3515	49,5	77,6952
15	21,2	1,1781303	3,228	1,56175	58	91,0368
16	21,2	1,1781303	5,004	1,78375	67	105,1632
17	21,2	1,1781303	6,804	2,00875	76	119,2896
18	21,2	1,1781303	8,655	2,240125	86	134,9856



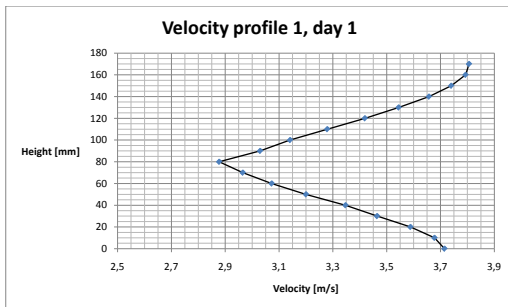
(a) Calibration 1



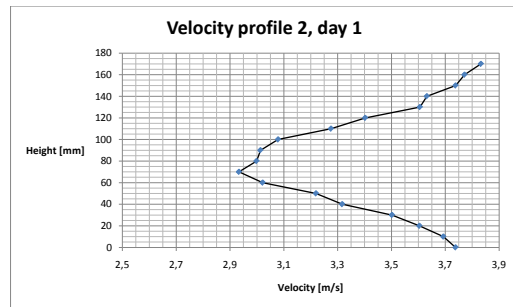
(b) Calibration 2

Figure A.1: Calibrations Day 1

For the measurements of the velocity profile day 1, the temperature was not logged. Therefore it was not possible to use the real density of air, but an approximation of  $\rho_{air} = 1.2[kg/m^3]$  was utilized. The pressure was calculated using the calibration constant. Then the velocity was derived from  $U = \sqrt{\frac{2\Delta P}{\rho_{air}}}$ . Low fan efficiency is applied in the velocity profile measurements for this day, and the same profile is measured twice. The vertical velocity profile behind the cylinder for low velocities in the test section is displayed in figure A.2. The data for these velocity plots can be found in table A.3 and A.4 for the first and second profile respectively.



(a) Vertical profile 1



(b) Vertical profile 2

Figure A.2: Vertical velocity profiles for the same velocity day 1

As can be seen the two graphs in figure A.2 does not display the same values for the vertical velocity profile. There can be several causes for these differences. The temperature probably rises due to the fan on the wind turbine. This will affect the air density and again the velocity. Still the temperature rise will not be big enough to cause large differences in the velocity. Inaccuracy in the positioning of the pitot tube can be another reason for the differing in the velocity profiles. This was done

Table A.3: Velocity profile 1, day 1

<b>H[mm]</b>	<b>E [V] 1</b>	<b>(E1-E0)/gain</b>	<b>Pdyn [Pa]</b>	<b>Velocity[m/s]</b>
0	-8,163	0,138125	8,28059375	3,7149683
10	-8,185	0,135375	8,11573125	3,6778008
20	-8,237	0,128875	7,72605625	3,5884203
30	-8,307	0,120125	7,20149375	3,4644609
40	-8,371	0,112125	6,72189375	3,3471116
50	-8,448	0,1025	6,144875	3,2002278
60	-8,512	0,0945	5,665275	3,0728040
70	-8,564	0,088	5,2756	2,9652431
80	-8,605	0,082875	4,96835625	2,8776020
90	-8,533	0,091875	5,50790625	3,0298256
100	-8,478	0,09875	5,9200625	3,1411416
110	-8,407	0,107625	6,45211875	3,2792577
120	-8,332	0,117	7,01415	3,4191007
130	-8,262	0,12575	7,5387125	3,5446467
140	-8,197	0,133875	8,02580625	3,6573684
150	-8,148	0,14	8,393	3,7400980
160	-8,116	0,144	8,6328	3,7931517
170	-8,108	0,145	8,69275	3,8062996

Table A.4: Velocity profile 2, day 1

<b>H[mm]</b>	<b>E [V] 2</b>	<b>(E2-E0)/gain</b>	<b>Pdyn [Pa]</b>	<b>Velocity[m/s]</b>
0	-8,149	0,139875	8,38550625	3,7384279
10	-8,176	0,1365	8,183175	3,6930509
20	-8,228	0,13	7,7935	3,6040486
30	-8,286	0,12275	7,3588625	3,5021094
40	-8,387	0,110125	6,60199375	3,3171257
50	-8,438	0,10375	6,2198125	3,2196823
60	-8,537	0,091375	5,47793125	3,0215700
70	-8,579	0,086125	5,16319375	2,9334830
80	-8,548	0,09	5,3955	2,9987497
90	-8,541	0,090875	5,44795625	3,0132917
100	-8,509	0,094875	5,68775625	3,0788948
110	-8,409	0,107375	6,43713125	3,2754468
120	-8,341	0,115875	6,94670625	3,4026230
130	-8,227	0,130125	7,80099375	3,6057809
140	-8,212	0,132	7,9134	3,6316662
150	-8,149	0,139875	8,38550625	3,7384279
160	-8,129	0,142375	8,53538125	3,7716886
170	-8,092	0,147	8,81265	3,8324600

manually and may therefore be inexact. All the measurements were performed with a frequency of  $400Hz$  and during a time period of  $30sec$ . This gives 12000 samples for each measurement which should give accurate results.

## A.4 Day 2, 4/2 - 2011

Atmospheric pressure:

- $h_{mercury} = 756,1mm$
- $P_{atm} = 100475,30Pa$

The calibration plot for the second day can be seen in figure A.3, and the data in the table A.5.

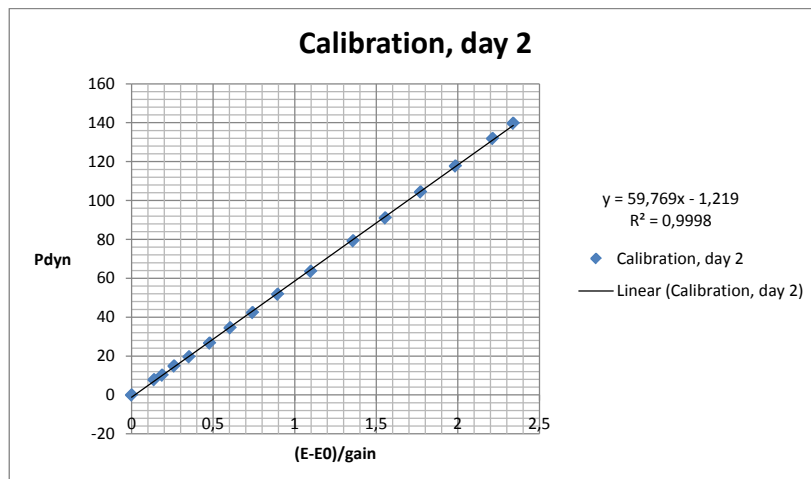


Figure A.3: Calibration Day 2

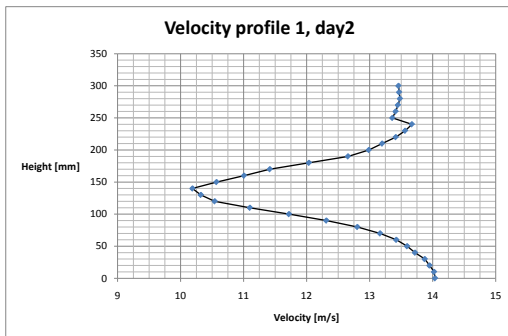
Two different vertical velocity profiles were measured. The profile from day 1 was for relatively low velocities, and therefore the fan efficiency was increased for the measurements during day 2.

While conducting the measurements for the first vertical velocity plot, it was noticed that the rubber tube from the pitot was clamped. It is obvious at the plot in figure A.4a where this was corrected. Therefore the measurements were done again, and these can be seen in figure A.5.

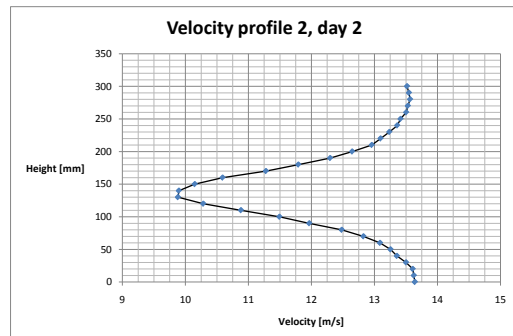
The values used to construct the two velocity plots A.2a and A.5 are displayed in the two tables A.3 and A.7 respectively.

Table A.5: Calibration 1, day 2

Nr	E [V]	Hx5 [mm]	Height [mm]	(E-E0)/gain	Pdyn	Tair [0C]
1	-9,345	0	0	0	0	18,6
2	-8,244	5	0,001	0,137625	7,848	18,7
3	-7,848	6,5	0,0013	0,187125	10,202	20,5
4	-7,262	9,5	0,0019	0,260375	14,911	20,8
5	-6,529	12,5	0,0025	0,352	19,62	21
6	-5,52	17	0,0034	0,478125	26,683	21,1
7	-4,514	22	0,0044	0,603875	34,531	21,2
8	-3,412	27	0,0054	0,741625	42,379	21,3
9	-2,181	33	0,0066	0,8955	51,797	21,3
10	-0,559	40,5	0,0081	1,09825	63,569	21,3
11	1,52	50,5	0,0101	1,358125	79,265	21,3
12	3,096	58	0,0116	1,555125	91,037	21,3
13	4,828	66,5	0,0133	1,771625	104,38	21,3
14	6,537	75	0,015	1,98525	117,72	21,3
15	8,363	84	0,0168	2,2135	131,85	21,3
16	9,373	89	0,0178	2,33975	139,69	21,3



(a) Vertical profile 1



(b) Vertical profile 2

Figure A.4: Vertical velocity profiles for the same velocity day 2

In theory the two plots should have the same velocity at the same heights. This was not the case for the plots from day 1 in figure A.2, and it is not the case for the two plots in figure A.4 either. The reason for the inaccuracy can be the same as mentioned for the differences in figure A.2 above.

A third vertical velocity plot was obtained during day two. The fan efficiency was lower than for the profiles in figure A.4, and higher than for those in A.2.

Table A.6: Velocity profile 1, day 2

Nr	H[mm]	E [V]	(E-E0)/gain	Pdyn[Pa]	Tair	rho_air	U [m/s]
1	0	6,353	1,96225	117,2822	294,3	1,19018	14,0386
2	10	6,314	1,957375	116,9908	294,4	1,18977	14,0236
3	20	6,146	1,936375	115,7357	294,5	1,18937	13,9505
4	30	5,977	1,91525	114,4731	294,5	1,18937	13,8742
5	40	5,64	1,873125	111,9553	294,5	1,18937	13,7208
6	50	5,366	1,838875	109,9082	294,5	1,18937	13,5948
7	60	4,992	1,792125	107,114	294,6	1,18897	13,4231
8	70	4,447	1,724	103,0422	294,6	1,18897	13,1655
9	80	3,697	1,63025	97,43882	294,7	1,18856	12,8047
10	90	2,714	1,507375	90,09467	294,7	1,18856	12,3127
11	100	1,58	1,365625	81,62238	294,7	1,18856	11,7195
12	110	0,454	1,224875	73,20986	294,7	1,18856	11,0991
13	120	-0,506	1,104875	66,03755	294,7	1,18856	10,5414
14	130	-0,873	1,059	63,29564	294,7	1,18856	10,3203
15	140	-1,089	1,032	61,68187	294,7	1,18856	10,1879
16	150	-0,459	1,11075	66,38869	294,7	1,18856	10,5694
17	160	0,291	1,2045	71,99206	294,7	1,18856	11,0064
18	170	1,021	1,29575	77,44601	294,7	1,18856	11,4157
19	180	2,18	1,440625	86,10508	294,7	1,18856	12,037
20	190	3,396	1,592625	95,19	294,7	1,18856	12,6561
21	200	4,071	1,677	100,233	294,7	1,18856	12,987
22	210	4,512	1,732125	103,5278	294,7	1,18856	13,1987
23	220	4,964	1,788625	106,9048	294,8	1,18816	13,4145
24	230	5,283	1,8285	109,2881	294,8	1,18816	13,5633
25	240	5,515	1,8575	111,0214	294,8	1,18816	13,6704
26	250	4,85	1,774375	106,0531	294,8	1,18816	13,361
27	260	4,96	1,788125	106,8749	294,8	1,18816	13,4127
28	270	5,037	1,79775	107,4502	294,8	1,18816	13,4487
29	280	5,107	1,8065	107,9732	294,8	1,18816	13,4814
30	290	5,079	1,803	107,764	294,8	1,18816	13,4683
31	300	5,056	1,800125	107,5921	294,8	1,18816	13,4576

Table A.7: Velocity profile 2, day 2

Nr	H[mm]	E [V]	(E-E0)/gain	Pdyn [Pa]	Tair	rho_air	U [m/s]
1	0	5,532	1,859625	111,1484	293,2	1,19465	13,641
2	10	5,487	1,854	110,8122	293,4	1,19383	13,625
3	20	5,447	1,849	110,5133	293,4	1,19383	13,6066
4	30	5,208	1,819125	108,7277	293,6	1,19302	13,5009
5	40	4,901	1,78075	106,4341	293,5	1,19342	13,3554
6	50	4,687	1,754	104,8353	293,5	1,19342	13,2547
7	60	4,336	1,710125	102,2129	293,5	1,19342	13,0879
8	70	3,787	1,6415	98,11122	293,6	1,19302	12,8248
9	80	3,095	1,555	92,94118	293,5	1,19342	12,4802
10	90	2,095	1,43	85,47003	293,4	1,19383	11,966
11	100	1,204	1,318625	78,81323	293,5	1,19342	11,4926
12	110	0,113	1,18225	70,6622	293,5	1,19342	10,8821
13	120	-0,897	1,056	63,11633	293,5	1,19342	10,2846
14	130	-1,545	0,975	58,27502	293,5	1,19342	9,88232
15	140	-1,521	0,978	58,45433	293,5	1,19342	9,89751
16	150	-1,115	1,02875	61,48762	293,4	1,19383	10,1493
17	160	-0,387	1,11975	66,92662	293,5	1,19342	10,5905
18	170	0,818	1,270375	75,92936	293,4	1,19383	11,2784
19	180	1,766	1,388875	83,01202	293,4	1,19383	11,7927
20	190	2,737	1,51025	90,26651	293,4	1,19383	12,2972
21	200	3,433	1,59725	95,46643	293,4	1,19383	12,6465
22	210	4,068	1,676625	100,2106	293,4	1,19383	12,9569
23	220	4,359	1,713	102,3847	293,4	1,19383	13,0967
24	230	4,653	1,74975	104,5812	293,4	1,19383	13,2364
25	240	4,918	1,782875	106,5611	293,4	1,19383	13,3611
26	250	5,031	1,797	107,4053	293,4	1,19383	13,4139
27	260	5,223	1,821	108,8398	293,4	1,19383	13,5032
28	270	5,28	1,828125	109,2657	293,4	1,19383	13,5296
29	280	5,357	1,83775	109,8409	293,4	1,19383	13,5652
30	290	5,319	1,833	109,557	293,4	1,19383	13,5476
31	300	5,252	1,824625	109,0565	293,4	1,19383	13,5167

Table A.8: Velocity profile 3, day 2

Nr	H[mm]	E [V]	(E-E0)/gain	Pdyn [Pa]	Tair	rho_air	U [m/s]
1	0	-2,658	0,835875	49,95962	291,7	1,20079	9,12202
2	10	-2,651	0,83675	50,01192	292,9	1,19587	9,14555
3	20	-2,7	0,830625	49,64583	293,1	1,19505	9,11513
4	30	-2,776	0,821125	49,07803	293,1	1,19505	9,06285
5	40	-2,928	0,802125	47,94241	293,2	1,19465	8,95892
6	50	-3,05	0,786875	47,03093	293,2	1,19465	8,87334
7	60	-3,173	0,7715	46,11198	293,2	1,19465	8,78623
8	70	-3,377	0,746	44,58786	293,2	1,19465	8,6398
9	80	-3,622	0,715375	42,75743	293,2	1,19465	8,4606
10	90	-4,031	0,66425	39,70172	293,3	1,19424	8,15407
11	100	-4,525	0,6025	36,01097	293,3	1,19424	7,76582
12	110	-4,994	0,543875	32,507	293,3	1,19424	7,37833
13	120	-5,454	0,486375	29,07027	293,2	1,19465	6,97622
14	130	-5,831	0,43925	26,25364	293,3	1,19424	6,63078
15	140	-5,827	0,43975	26,28353	293,3	1,19424	6,63455
16	150	-5,796	0,443625	26,51513	293,3	1,19424	6,66372
17	160	-5,592	0,469125	28,03925	293,3	1,19424	6,85256
18	170	-5,004	0,542625	32,43229	293,2	1,19465	7,36859
19	180	-4,561	0,598	35,74201	293,2	1,19465	7,73544
20	190	-4,147	0,64975	38,83507	293,2	1,19465	8,0632
21	200	-3,752	0,699125	41,78618	293,2	1,19465	8,36396
22	210	-3,427	0,73975	44,2143	293,3	1,19424	8,605
23	220	-3,302	0,755375	45,1482	293,2	1,19465	8,69392
24	230	-3,116	0,778625	46,53783	293,2	1,19465	8,82671
25	240	-2,978	0,795875	47,56885	293,3	1,19424	8,92547
26	250	-2,948	0,799625	47,79299	293,2	1,19465	8,94494
27	260	-2,794	0,818875	48,94354	293,2	1,19465	9,05197
28	270	-2,743	0,82525	49,32457	293,2	1,19465	9,08714
29	280	-2,731	0,82675	49,41423	293,3	1,19424	9,09695
30	290	-2,763	0,82275	49,17515	293,3	1,19424	9,07491
31	300	-2,766	0,822375	49,15274	293,3	1,19424	9,07284



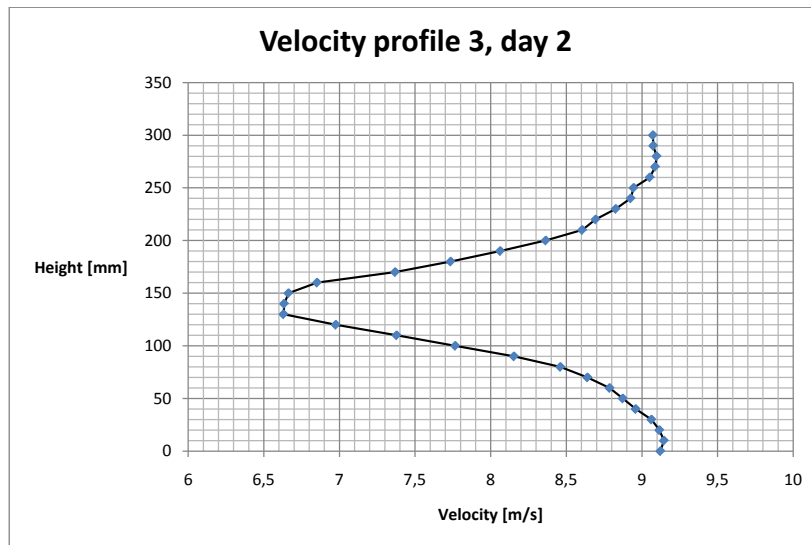


Figure A.5: Vertical velocity profile day 2

The aim of this task was to learn how to use the equipment necessary for conducting experiments in a wind tunnel. This was accomplished during the days in the small wind tunnel. Knowledge of how to process the data obtained was also achieved. The results should be discussed and analyzed at a higher level than what is done here, in an experiment where the aim is to require and understand the measurement data obtained.

## B Calibration

The calibrations are done several times for the various instruments. This is because the measurements were conducted at different times, often with several weeks parting the periods spent in the wind tunnel. One calibration curve for each of the instruments calibrated is shown here.

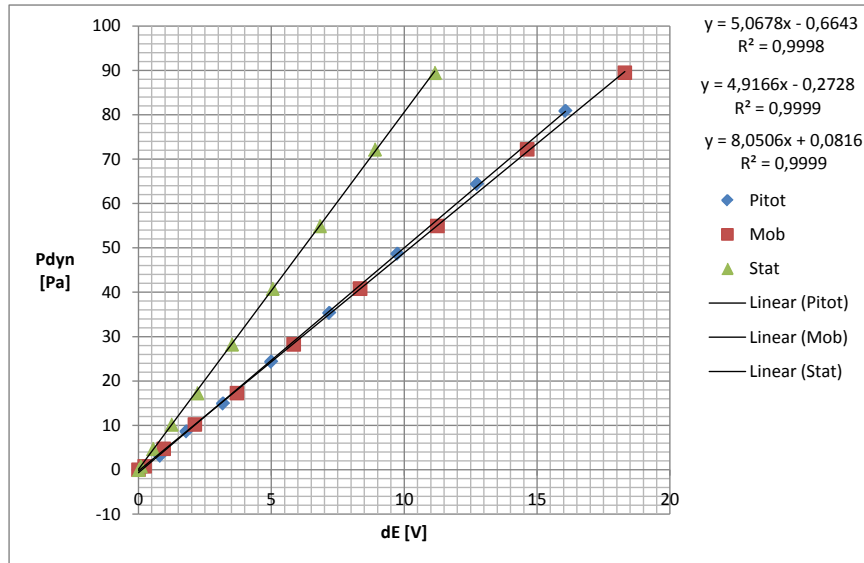


Figure B.1: Calibration of the pressure transducers used for measuring pitot tube pressure, reference pitot pressure at the test section entrance and the contraction pressure(stat)

Figure B.1 shows the calibration curves for the three different pressure transducers used in the measurements. The pitot tube is connected to a pressure transducer and the calibration curve is named Pitot. As mentioned in the thesis there is a pitot tube placed at the entrance of the tunnel test section. This is called the reference pitot, and the calibration curve for the pressure transducer connected to the reference pitot tube is called Mob in figure B.1. The calibration curve marked Stat is for the contraction and the stationary pressure transducer connected to the measure points here. Theoretical pressure calculated from the gravity constant, density and height of Methylated spirit is plotted against the voltage differences for the various pressure transducers. This gives a calibration constant with the unit  $[\frac{Pa}{V}]$ , and the pressure can then in tests be found by multiplying the voltage obtained with the calibration constant.

The torque calibration curve is displayed in figure B.2. Theoretical torque found by multiplying the gravity constant with applied weight and arm is plotted against

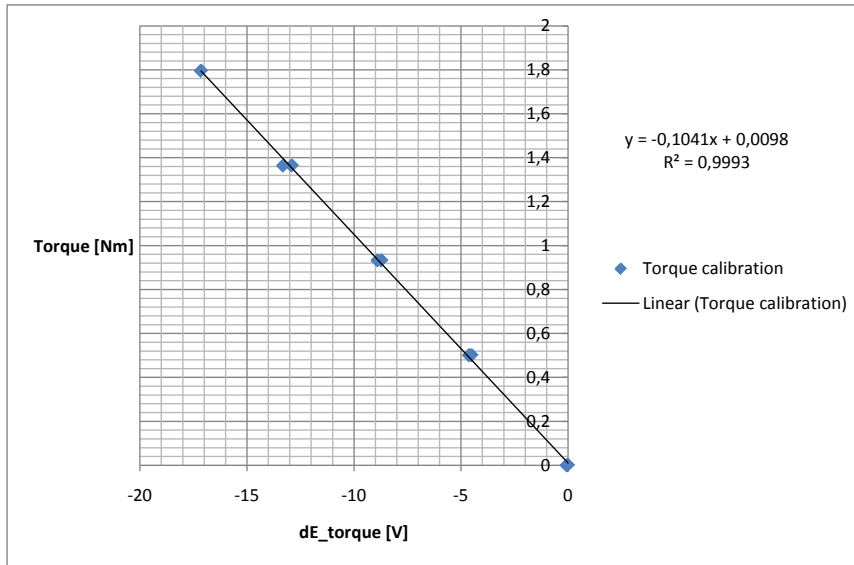


Figure B.2: Torque calibration

the voltage measured for the different moments. The slope of the calibration curve gives the calibration constant in  $[\frac{Nm}{V}]$ . Then when measuring torque this constant is multiplied with the voltage obtained and gives the torque for this case.

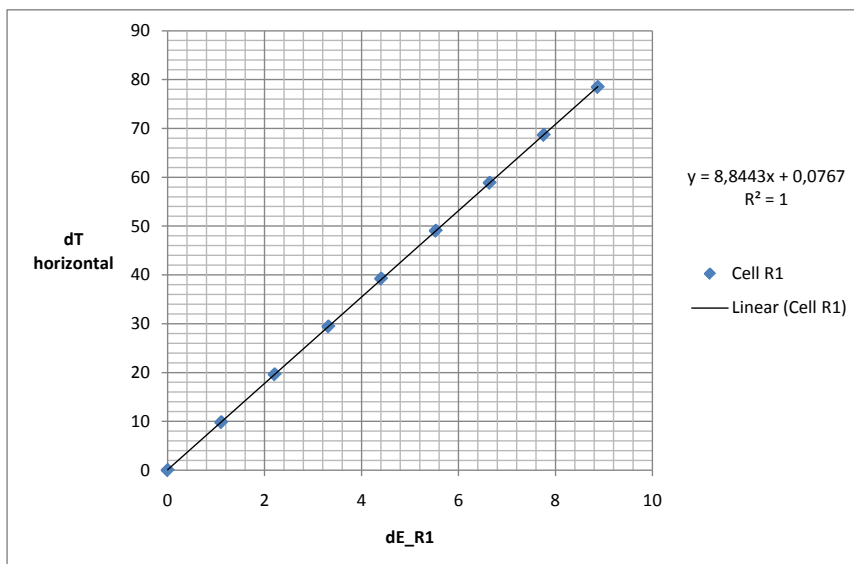


Figure B.3: Calibration of the vertical balance cell R1

The balance consists of six different load cells. They are all calibrated the same

way, but with different gains and calibration constants. Here the calibration curve for the cell R1 is displayed. Weight applied multiplied by the gravity constant is plotted against the voltage, and this gives the calibration constant in  $[\frac{N}{V}]$

The amplifier gains for the different calibration curves are not taken in to consideration here. That is because a new calibration has been done for each time period the tests have been performed, and therefore it will give the same result if the gain is taken in to the result calculations or not. The gains used for the calibration and measurements can be found on the DVD with the measurement data belonging to this thesis on. If the gain is changed after calibrating the instrument, it is necessary to bring this factor in to the calculation of the calibration constant and the results.

The rest of the calibration curves, calculations and values can be found on the disc following this thesis.

## C Measurement data

For each of the grid measurement performed in this thesis, the vertical velocity profile was documented. This was mainly done to have a method of comparing the grid measurement with a separate set of data and thus being able to validate the results. For the cases where the yaw angle is zero,  $\gamma = 0$ , only one vertical profile is measured. There are done two separate measurements for the the wind turbine when it is operating in oblique inflow. The one where  $x = 0$  represents the vertical profile behind the center of the hub. When  $x = 67.5mm$  the vertical profile is measured behind the location of the tower. The tower location after the rotation of the wind turbine is found by geometry. See figure C.1.

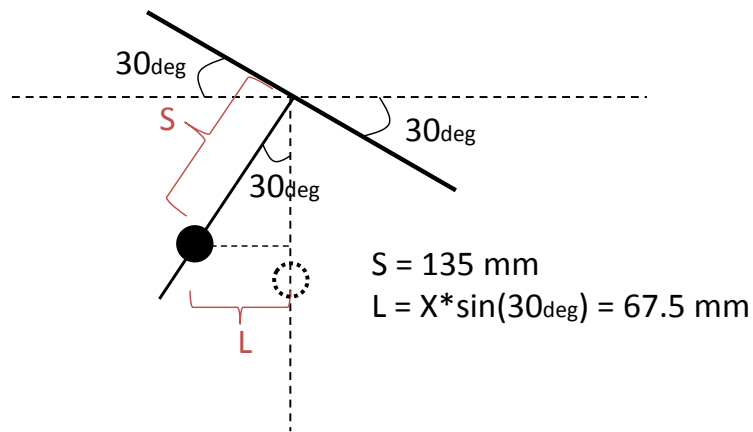
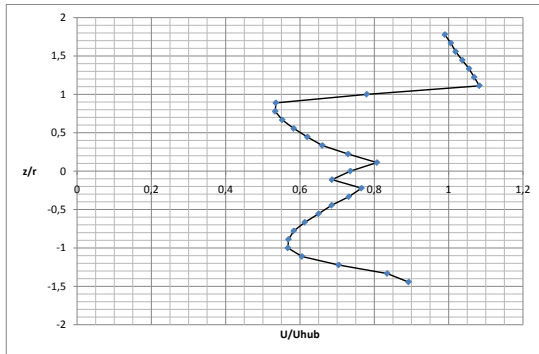
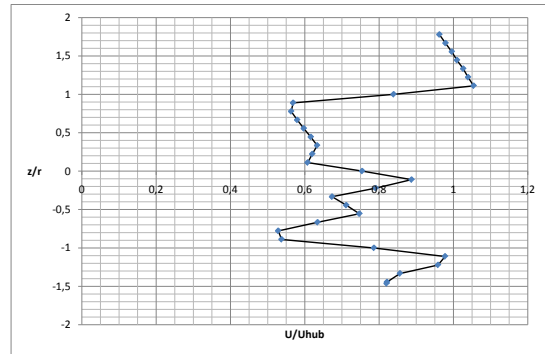


Figure C.1: Position of the tower when the turbine is rotated  $30^{\circ}$

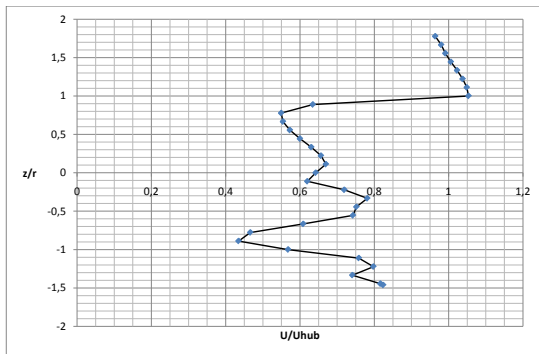
For the profile in figure C.2 the vertical profile is also measured at a position  $x = 80mm$ , see figure C.2d. It was originally planned to perform this measurement for all the cases, but it was found to be unnecessary and time consuming. Therefore this vertical profile only appears for  $TSR = 6$  and  $\gamma = 30^{\circ}$ .



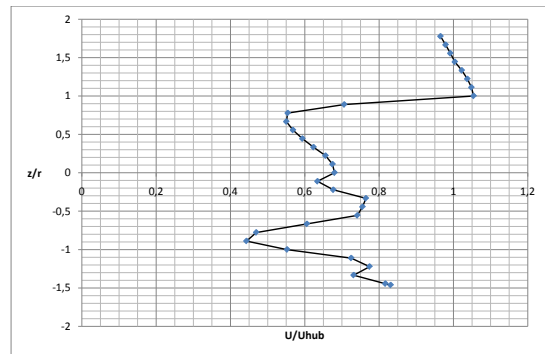
(a)



(b)

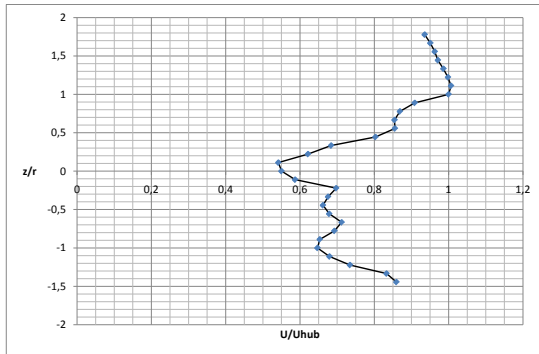


(c)

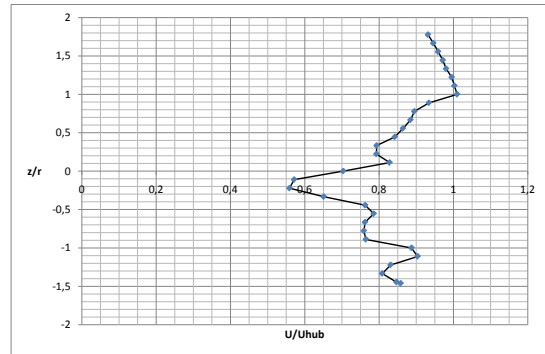


(d)

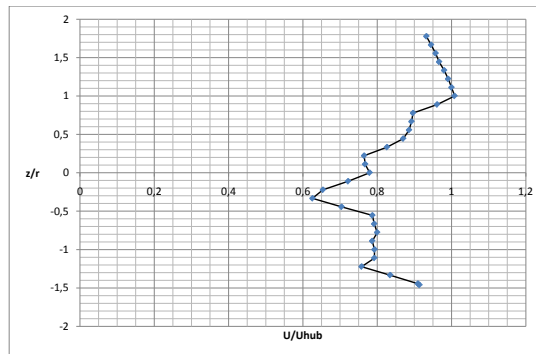
Figure C.2: Vertical profiles for different yaw angles at  $X/D = 1$  behind the rotor plane for  $TSR = 6$  where a)  $\gamma = 0^\circ$  and  $x = 0mm$ , b)  $\gamma = 30^\circ$  and  $x = 0mm$ , c)  $\gamma = 30^\circ$  and  $x = 67.5mm$ , d)  $\gamma = 30^\circ$  and  $x = 80mm$



(a)

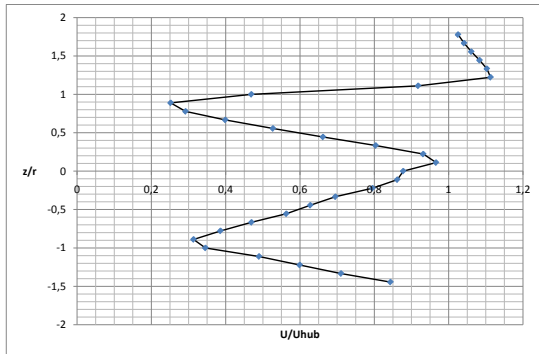


(b)

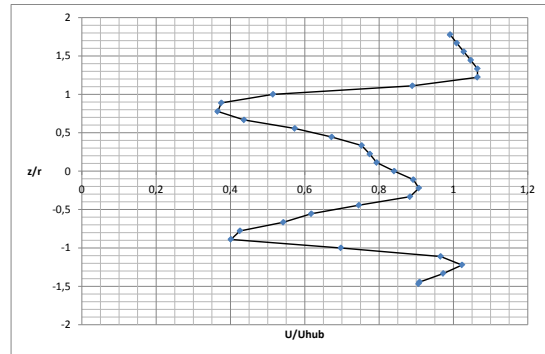


(c)

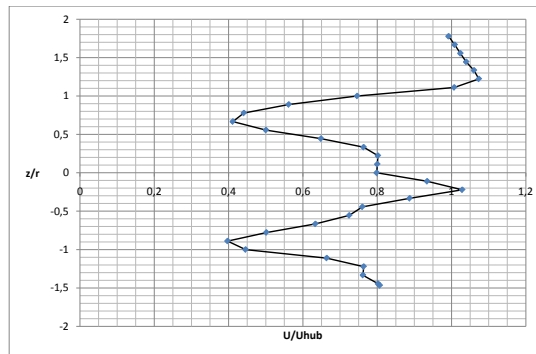
Figure C.3: Vertical profiles for different yaw angles at  $X/D = 1$  behind the rotor plane for  $TSR = 3$  where a)  $\gamma = 0^\circ$  and  $x = 0mm$ , b)  $\gamma = 30^\circ$  and  $x = 0mm$ , c)  $\gamma = 30^\circ$  and  $x = 67.5mm$



(a)



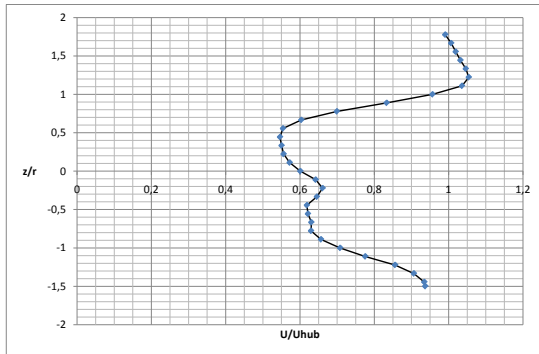
(b)



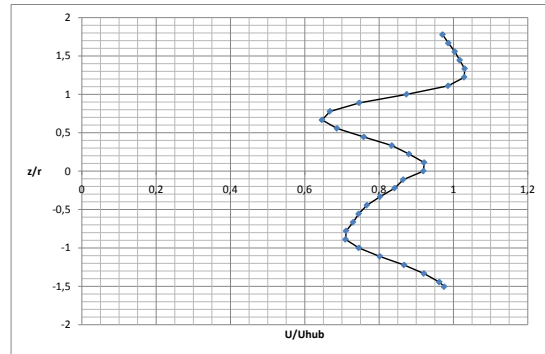
(c)

Figure C.4: Vertical profiles for different yaw angles at  $X/D = 1$  behind the rotor plane for  $TSR = 9$  where a)  $\gamma = 0^\circ$  and  $x = 0mm$ , b)  $\gamma = 30^\circ$  and  $x = 0mm$ , c)  $\gamma = 30^\circ$  and  $x = 67.5mm$

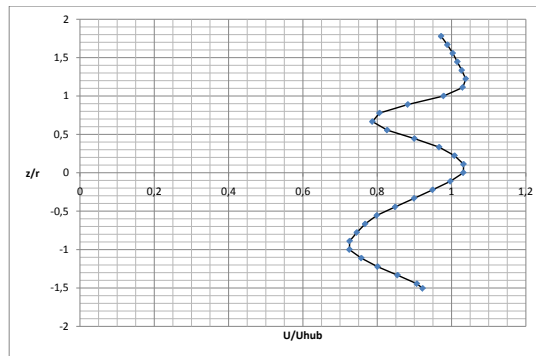




(a)



(b)



(c)

Figure C.5: Vertical profiles for different yaw angles at  $X/D = 4$  behind the rotor plane for  $TSR = 6$  where a)  $\gamma = 0^\circ$  and  $x = 0mm$ , b)  $\gamma = 30^\circ$  and  $x = 0mm$ , c)  $\gamma = 30^\circ$  and  $x = 67.5mm$